Republic of Iraq

Ministry of Higher Education & Scientific Research

University of Kerbala

College of Engineering

Civil Engineering Department

Shear Friction Strength of Ultra- High Performance Concrete Construction Joints

A Thesis Submitted to the Council of the Faculty of Engineering/University of Kerbala in Partial Fulfillment of the Requirements for the Master Degree in Civil Engineering

Written by:

Ali Ahmed Abdulredha

Supervised by:

Assist Prof. Dr. Bahaa Al-Abbas

Prof. Dr. Sadjad A. Hemzah

2023 April   2023 Ramadan

بسم الله الرحمن الرحيم

يَرْفَعِ اللَّهُ الَّذِينَ آمَنُوا مِنكُمْ وَالَّذِينَ أُوتُوا الْعِلْمَ دَرَجَاتٍ
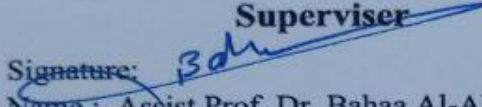
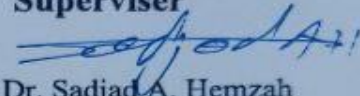صدق الله العلي العظيم

(المجادلة: من الآية 11)

Examination committee certification

We certify that we have read the thesis entitled "**Shear Friction Strength of Ultra High Performance Concrete Construction Joints** " and as an examining committee, we examined the student " **Ali Ahmed Abdulredha**" in its content and in what is connected with it and that in our opinion it is adequate as a thesis for the degree of Master of Science in Civil Engineering.
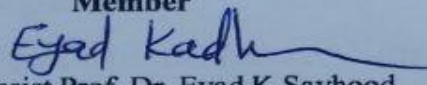
Superviser

Signature:

Name :. Assist Prof. Dr. Bahaa Al-Abbas

Date: / / 2023

Superviser

Signature:

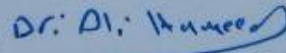Name :. Prof. Dr. Sadjad A. Hemzah

Date: / / 2023

Member

Signature:

Name :. Assist Prof. Dr. Eyad K.Sayhood

Date: / / 2023

Member

Signature:

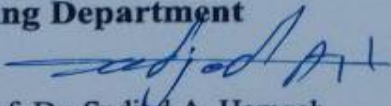Name :. Assist Prof. Dr. Wajde S.S Alyhya

Date: 16 /4 / 2023

Chairman

Signature: Dr. Ali Hameed

Name :. Prof. Dr. Ali Hameed Nasear

Date: 16 /4 / 2023

Approval of Head of Civil Engineering Department
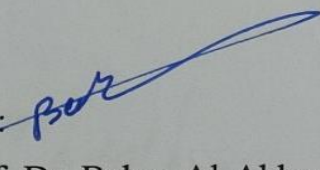
Signature:

Name : Prof. Dr. Sadjad A. Hemzah

Date: / / 2023

Approval of Deanery of the College of Engineering

Signature:

Name : Prof. Dr. Laith Shakir Rasheed

Date: / / 2023

II
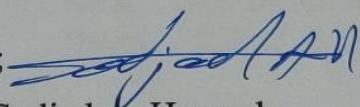
Supervisor certificate

We certify that the thesis entitled **"Shear Friction Strength of Ultra High Performance Concrete Construction Joints"** was prepared by **Ali Ahmed Abdulredha** under our supervision at the Department of Civil Engineering, Faculty of Engineering, University of Kerbala as a partial of fulfilment of the requirements for the Degree of Master of Science in Civil Engineering.

Signature:

Assist Prof. Dr. Bahaa Al-Abbas

Date: /   / 2023

Signature;

Prof. Dr. Sadjad A. Hemzah

Date: /   / 2023

III

Abstract

In this study, the shear friction behavior of UHPC was investigated both experimentally and numeircally by conducting tests on 9 push-off specimens using ultra-high performance concrete (UHPC). UHPC is distinguished from other types of concrete by lack of coarse aggregate, steel fiber reinforcing, low water-to-cement ratio, low permeability, compressive strength exceeding 120 MPa, and average tensile strength 10.77 MPa. To maximize the benefits of UHPC in joints, new model guidelines for its application are required. In order to employ hybrid design approaches with this novel material without putting anyones safety at risk, the contact between the UHPC has to be described. The major parameters considered are the types of interfacing and using of shear reinforcement through the shear plane. Key factors affecting shear performance of individual construction joint were investigated in terms of shear strength, failure mechanism, and slip responses.

The observations from experimental tests showed that the increase in the shear reinforcement improves shear resistance, The grooved interfacing wear was discovered to be a successful approach compeard to other interfacing techniques for increasing the shear capacity of a contact, in contrast to the exposed fibers specimens, which were shown to be ineffective in increasing the shear strength. The finite element method using (ABAQUS) was utilized to create a model for the structural behavior of push-off specimen. In terms of the maximum slip and the ultimate load capacity, the findings revealed that there was a good agreement between experimental and the numerical results. The mean differences in the ultimate load capacity were (7.56) %. Various new parameters were suggested to be investigated

numerically by the verified model, such as the number of dowel bars, and the concrete strength.

The numerical findings showed that increasing the number of dowel bars from one to two and from three to four was able to enhance the final load capacity by 23% and 14 %, respectively, in contrast with one dowel bar and three dowel bars . Furthermore, increasing the concrete strength from (120 to 200 MPa) had a clear performance and more efficient to obtain higher ultimate load by (59 and 60 %) for the specimens with rectangl and circular grooves respectively. Finally, an interaction formula for the shear friction strength was proposed on the basis of the experimental results, to predict the shear load-carrying capacity of the UHPC structures.

Undertaking

I certify that the research work titled "**Shear Friction Strength of Ultra-High Performance Concrete Construction Joints**" is my own work. The work has not been presented elsewhere for assessment. Where material has been used from other sources it has been properly acknowledged / referred.

Signature:

Ali Ahmed Abdulredha

Date: /   / 2023

Dedication

TO everyone helped me in this journey

Acknowledgements

In the name of **Allah**, the most gracious the most merciful.

Signature:

Ali Ahmed Abdulredha

Date: /   / 2023

Table of Contents

XII

List of Tables

List of Figures

List of Abbreviations

ACI	American concrete institute
AFGC	Association Francaise du Genil Civil
ASSHTO	American Association of State Highway and Transportation Officials
ASTM	American society for testing materials
CDP	Concrete damage plasticity
CGS	Circular grooves specimen
CS	Control specimen
DBS	Dowel bar specimen
EXF	Exposed fiber specimen
FEA	Finite element analysis
HPC	High performance concrete
ksi	Kilopound per square inch
LRFD	Load and resistance factor design
MPa	MegaPascal
NSC	Normal strength concrete
RGS	Rectangl grooves specimen
TGS	Triangl grooves specimen
UHPC	Ultra high performance concrete
W/B	Water to binder ratio

List of Symbols

Vu	The ultimate nominal shear transfer stress in kN
fy	The yield strength of the reinforcement steel in MPa
c	The cohesion associated with the concrete
ρv	The ratio of the shear reinforcement crossing the shear plane
σn	The permanent compressive stress in MPa
μ	fraction of concrete strength
τadh	adhesion bond in MPa
τsf	shear-friction in MPa
τsr	shear reinforcement in MPa
f_c'	Cylinderecal compressive strength of concrete at 28 days in MPa
E_s	Modulas of elasisty of steel reinforcement in MPa
A_{cv}	Area of concrete at the shear plane in mm^2
λ	The modification factor
ψ	Dialton angle
ϕ	Size of barBar diameter (mm)

CHAPTER ONE: INTRODUCTION

1.1 General

The problem of concrete-to-concrete load transfer arises when new concrete is cast against old concrete that has completed its hardening process. This could be useful in the following situations:

- ➢ Using new concrete sections to repair and reinforce existing RC elements.
- ➢ Using cast-in-place concrete to supplement prefabricated components.
- ➢ Construction joints connect concrete sections that have been cast in place one after the other.
- ➢ Load transfer is accomplished by attaching concrete elements (such as corbels) to existing members.

External tension stresses are transmitted across the interface through reinforcement, whereas compression stresses are transmitted directly through the concrete. The major purpose is to ensure that, based on the direction of the compression struts, shear forces are carried along the joint (Randl, 2013).

1.2 Shear Friction

Slipping along a crack in a reinforced concrete element will be difficult as concrete is rough and irregular. If a crack develops in a reinforced concrete element and the concrete pieces on the opposite sides of the crack are not allowed to move out, it will be hard to slip. If reinforcement is put across a crack to prevent it from moving in the opposite direction, friction between the faces will prevent shear, the concretes resistance to being cut off, not to mention the dowel-like action of the reinforcing that spans the crack.

(Zilch and Reinecke, 2000)characterized the shear capacity of concrete-to-concrete surfaces as the interplay of three load-carrying mechanisms: 1) adhesion bond, τadh; 2) shear-friction, τsf; and 3) shear reinforcement (dowel action), τsr. Each mechanisms effect on the shear transfer strength is broken out in Figure (1-1). To

putting it another way, adhesion-based shear strength may be thought of as the load being transferred from the fresh concrete particles to the old concrete through their chemical bonds. In contrast to shear friction and the dowel action, the adhesive bond is a hard sort of connection (Rahman and Hoque, 2019).

If shear friction is used, this means that the shear will move through it. Shear friction is more likely to fail in short, deep parts that are subjected to a lot of shears and small bending moments. Brackets, corbels, and precast connections are usually made with a design called shear friction. It can also be used to connect concrete that was made at different times and to connect concrete and steel sections. If the shear friction fails, Figure (1-2) and figure (1-3) shows how it could happen(McCormac and Brown, 2015).
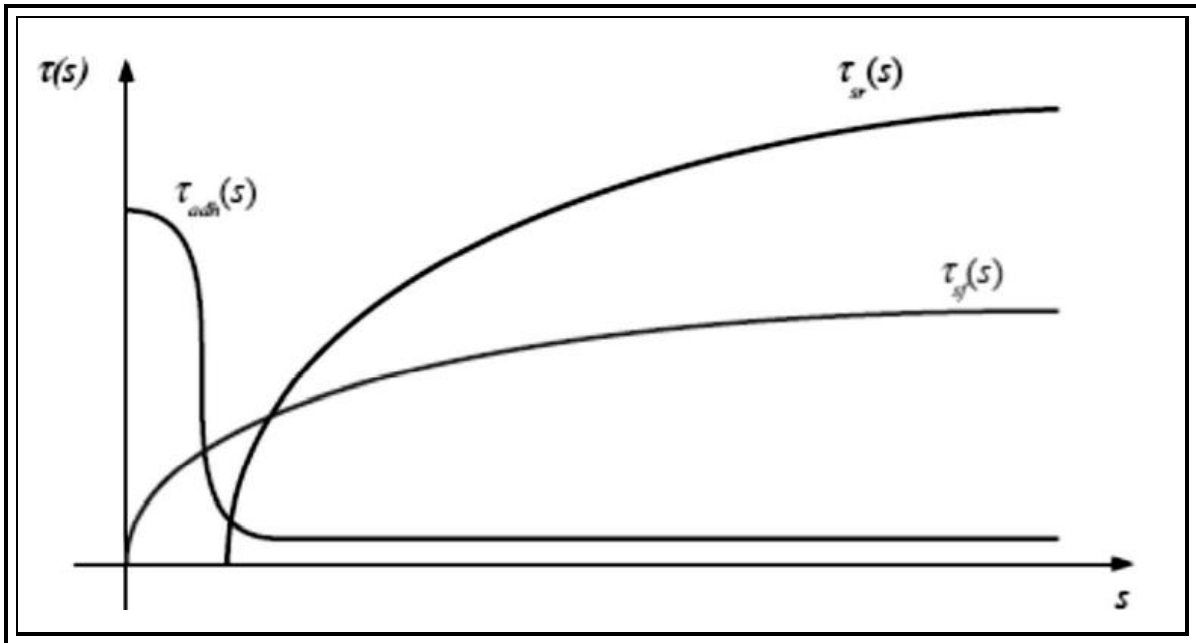
Figure 1- 1. Aspects of dowel force, shear friction, and adhesiveness (Rahman and Hoque, 2019)
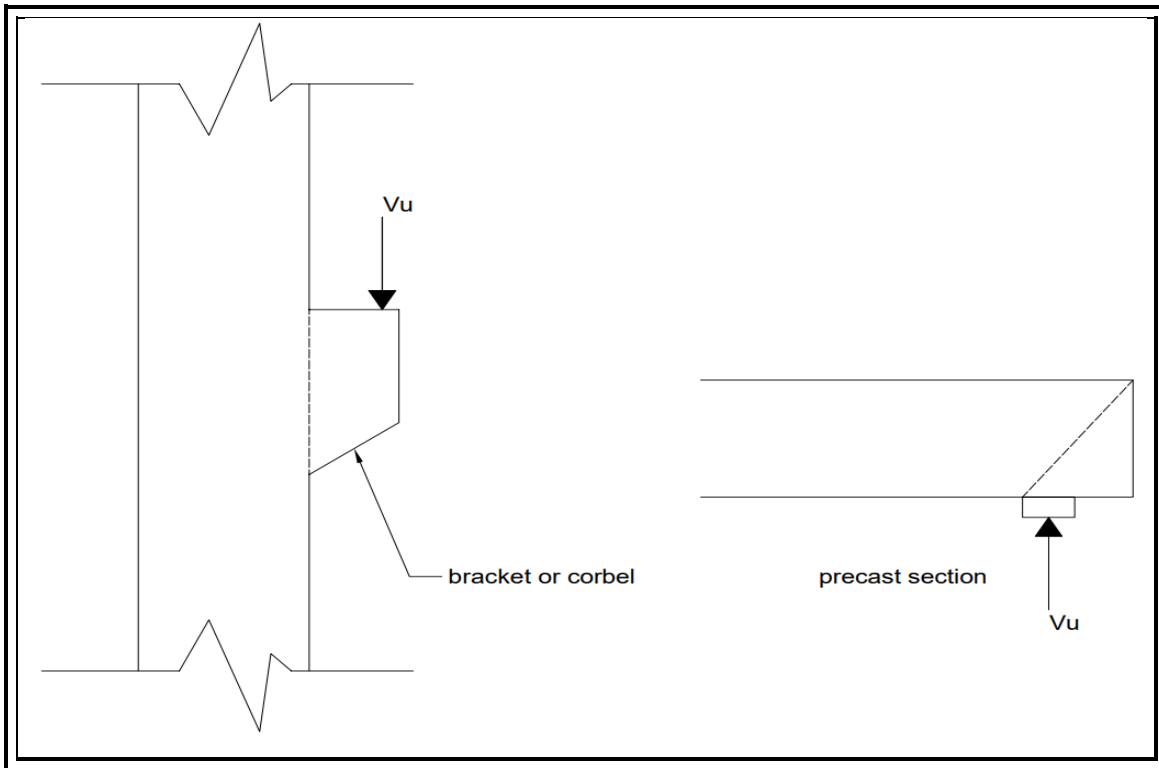
Figure 1- 2.Possible shear friction failure(McCormac and Brown, 2015).
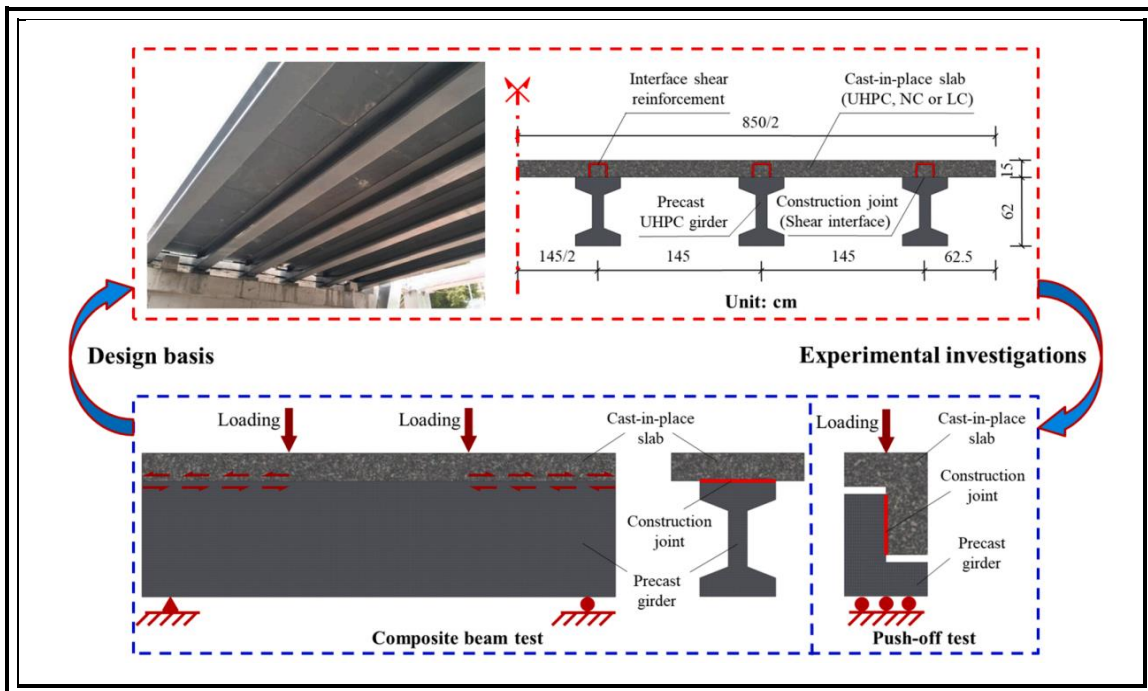
Figure 1- 3. Example of shear friction application(Jiang et al., 2021).

1.2.1 ACI and ASSHTO codes requirement for shear provision

In this part, it is shown how the design criteria for shear transfer strength differ among the most used design codes. Each codes drawbacks and requirements are described in detail as well.

1.2.1.1 ACI 318-19

Birkeland and Birkeland (1966) and Mast (1968), came up with the idea of shear friction. The ACI code 318-19, and its commentary, ACI 318R-19, used the unique version of this philosophy. Clause 22.9.4.2 of the ACI 318-19 says that friction is the only thing that affects the ultimate nominal shear transfer resistance as follows:

$$Vn = \mu A_{vf} fy \qquad\qquad 1\text{-}1$$

Where Avf is the area of reinforcment crossing the assumed shear plane, μ is the coefficient of fraction, and fy is the yield stresse of reinforcement.

In ACI 318-19, clause 22.9.4.2, it could be seen that the coefficient of friction is determined by the state and preparation of the contact plane, as shown in Table 1.1. This table says that normal-weight concrete should have a density modification factor of 1.00, and all lightweight concrete should have a density modification factor of 0.75, which is the same for all of them. Lightweight and normal-weight aggregates are used to figure out the volumetric proportions. It canot be more than 0.85%.

Table1.1 Coefficient of friction, μ proposed by ACI 318 (2019).

Surface condition	μ
Monolithic Concrete.	1.4λ
Concrete poured up against freshly poured, laitance-free, and purposefully roughened 0.25 in (6.35 mm).	1.0λ
Concrete affixed on smooth, laitance-free, previously cured concrete that has not been purposefully roughened.	0.6λ
Placement of pure, unpainted as-rolled structural steel with headed shear studs or welded deformed bars or wires across which concrete is then laid.	0.7λ

1.2.1.2 AASHTO LRFD Bridge Design Specifications (2017)

Specifications for bridge building according to AASTHO LFRD (2017), in accordance with subsection 5.7.4 of this code, shear transfer across a specific plane must be taken into account when: (a) a preexisting or developing fracture; (b) a transition between materials; (c) a transition among concretes poured at various periods; and (d) a transition between parts of a cross section. To create these scenarios, the modified shear friction equation is employed (Mattock and Hawkins, 1972), which takes into consideration the interface cohesiveness of the concrete contact. Vu is the final nominal shear transfer stress calculated as follows:

$$Vni = cAcv + \mu(Avffy + Pc) \hspace{2cm} 1\text{-}2$$

in which μ is the friction factor, fy is the yield strength of the steel [capped at 60 ksi (414 MPa)], c is the cohesion linked with an interfaces concrete plane, Avf is the area of the reinforcement crossing vertical to the interface, and Pc is the enduring

compressive stress normal to the shear plane (zero if tension). According to Table 1.2, the code specifies the proportion of concretes strength available to withstand the interface shear K1(concrete cohesion term that is related to strength), as well as the factor K2(maximum allowable interface stress), c, and for different circumstances of the substrate interface.

1.3 Ultra-High Performance concrete (UHPC)

UHPC Is a type of concrete mixture with strength equla to or more than 120 MPa that becomes more popular and take place in the present study (C1856/C1856M-17, 2017). In comparison to conventional cement-based materials, UHPC typically has a high concentration of steel fiber reinforcing that is sperate randomly through it, which contributes to the new tensile stress and strain responses, silica fume and ultra-fine silica powder are widely used in the matrix composition of UHPC to improve the particle system's packing density, hence increasing the materials strength (Al-Azzawi et al., 2011). The tensile cracking strength is (8-17 MPa) and the tensile cracking strength is sustained, via the discontinuous internal fiber reinforcement. The modulus of elasticity is usually within the range of 6000 to 8000 ksi (41 to 55 GPa) (Haber et al., 2018). More cementitious ingredients. A sufficient amount of a superplasticizer to assure the generated matrixs fluidity and viscosity. The tensile and spalling resilience of the matrix is improved by blending fibers. Because UHPC has so many advantages, its popularity has risen gradually since its introduction(Akhnoukh and Buckhalter, 2021). For instance, UHPC is now commonly used in structures such as buildings, highways, bridges, and other structures.

Table 1.2 Values of c, μ and factors $k1$ and $k2$ according to AASHTO LFRD (2017).

Interface condition	c	μ	k_1	k_2
cast-in-place concrete slab placed against hardened, clean and roughened to an amplitude of 0.25 in surface of a concrete girder	0.28 ksi	1.0	0.30	1.8 ksi for normal concrete 1.3 ksi for lightweight concrete
normal monolithic concrete.	0.4 ksi	1.4	0.25	1.5 ksi
Intentionally roughened to an amplitude of 0.25 in., lightweight concrete may be used in either a monolithic or non-monolithic installation.	0.24 ksi	1	0.25	1.0 ksi
normal concrete on a freshly roughened concrete block measuring 0.25 inches in height.	0.24 ksi	1	0.25	1.5 ksi
Placement of concrete vs a smooth, non-roughened concrete surface.	0.075 ksi	0.6	0.2	0.8 ksi
Anchored concrete with pure, unpainted as-rolled structural steel, either by headed studs or reinforcing bars.	0.025 ksi	0.7	0.2	0.8 ksi

1.4 Research Aim

The main goal of this work is to inspect the effects of using UHPC on the shear fraction strength of construction joint. The main purposes of this study are summarized as follows:

- ➢ To investigate the shear friction behavior of UHPC assembly joins in an experimental setting.
- ➢ Numerical results are compared to existing experimental results to ensure that the numerical techniques used and proposed member and material models are valid.

1.5 Thesis Layout

This thesis presented in six chapters.

- ➢ The first chapter gives a general overview of shear friction, including how to use UHPC and different types of surfaces.
- ➢ The second chapter explains how to review the existing literature for this study.
- ➢ Chapter three descripe the experimental work, properties of materials, configuration and testing procedure.
- ➢ The fourth chapter clarifies the experimental results and their discussion.
- ➢ The fifth chapter demonstrates how to use finite element analysis to develop a validated model that can accurately forecast the new case studies given.
- ➢ The study results and recommendations for further work are presented in the sixth chapter.

Chapter Two: Literature Review

2.1 Introduction

In reinforced concrete structures, there are instances where the transfer of shear stresses along a definite plane needs to be considered. Such cases include Connections between concrete layers cast at different times, which exist in wide range of structural applications, such as composite construction of precast and cast-in-situ concrete structures. (Hofbeck et al., 1969) and (Mattock and Hawkins, 1972) have been the first to examine the shear transmission between initially uncracked shear planes in monolithic concrete.The majority of the past investigations into the shear rubbing issue were conducted in view of the test after effects of push-off examples. (Anderson, 1960, Hanson, 1960) were the first to present these specimens, and they have been widely utilized since then. This type of specimen has been shown to be good at simulating how joints work in composite concrete structures in the real world.

2.2 Previous research on UHPC shear friction

Jang et al. (2018) Evaluate the shear performance of plain UHPC construction joints in both experimentaly and analyticaly. The push-off experiment was carried out for three distinct configurations of a construction joint integrated with 180 MPa UHPC, with a reference example of solid UHPC pouring indicated in Figure (2-1). The cracking and the connection between vertical slip and shear bond strength for each specimen are studied using experimental findings. It was found that the maximum ultimate stress for the monolithic casting case was 20.80 MPa with interfacial failure and substrate cracks, the shear stresses capacity for the longitudinal joint case was 0.72 MPa with complete interfacial failure, and the maximum shear strength for the grooved joint cases is 16.05 MPa for rectangle groove 30mm (GR-30). A standardized finite-element analysis method in three dimensions was included in the paper. There were three potential causes of failure that are examined in detail: (a) damaged plasticity in the plain UHPC substrate, (b) friction in horizontal contact surfaces, and (c) cohesive failure in vertical contact surfaces. The ultimate shear force, failure mechanism, and

dislocation reactions. In terms of slip responses, maximum shear strength, and mode of failure, all of the generated simulation solutions were in good agreement with tests. The laterally command increases the height of the shear key in both dry and cast –in –place joints.
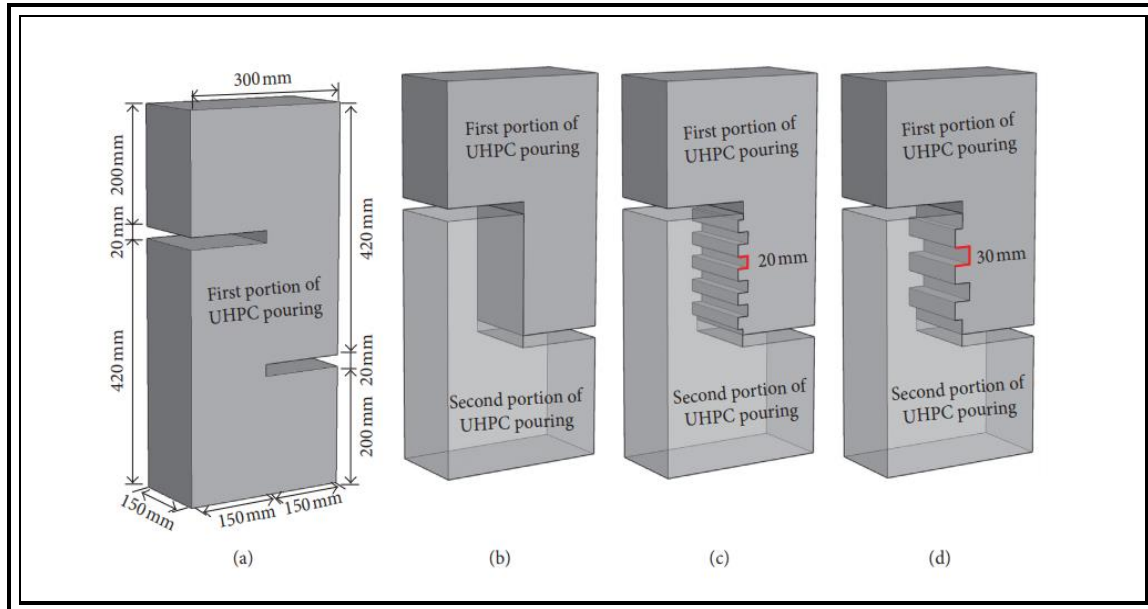
Figure 2- 1. Configuration of each specimen(16). (a) refrance (b) virtical joint (c) 20 mm rectangle grooves (d) 30 mm rectangle grooves

Liu et al. (2019) study the Precast segmental bridges made of ultrahigh-performance concrete (UHPC) using total of 25 specimens of concrete dry joints were tested, including 4 flat joints, 10 single-keyed joints, 8 three-keyed joints, and 3 large-keyed joints as shown in Figure (2.2) . Shear transmission at dry joints between UHPC segments is a major source for worry as a result of cracks and holes in the reinforced bars. The shear resistance of UHPC joints should have been tested for this study. Keys were examined, as were the shape and size of joints, the location of reinforcement, and the amount of stress that could be applied to each joint. Normalized shear stress-relative slip graphs characteristic of the material were produced, as were brittle fracture processes, cracking patterns, ultimate shear load, and vertical slippage. In this study, increasing the confined stress, the tensile strength of the matrices, and the presence of steel fibers in UHPC joints all contributed to an increase in shear resistance. When comparing fiber-reinforced concrete joints to conventional joints, the former were far

less likely to show signs of concrete crushing in the joint region. The shear force of large-keyed joints was 9.7 percent higher than that of three-keyed joints. It was determined how to determine the shear strength of concrete dry joints using Mohr's circle, and a simpler formula was created for determining the shear strength of UHPC dry joints of varying compressive strengths.

Good agreement was established between the calculated values and the measured result using the suggested technique of computation. With a standard deviation of 0.14, the average ratio of numirical to experimental data was 1.01. With an average ratio of 0.96 and a standard deviation of 0.24, the reduced equation for UHPC joints was determined to be in greater accord with the shear test findings than the AASHTO requirements, which had a ratio of 1.41 and a variance of 0.38.
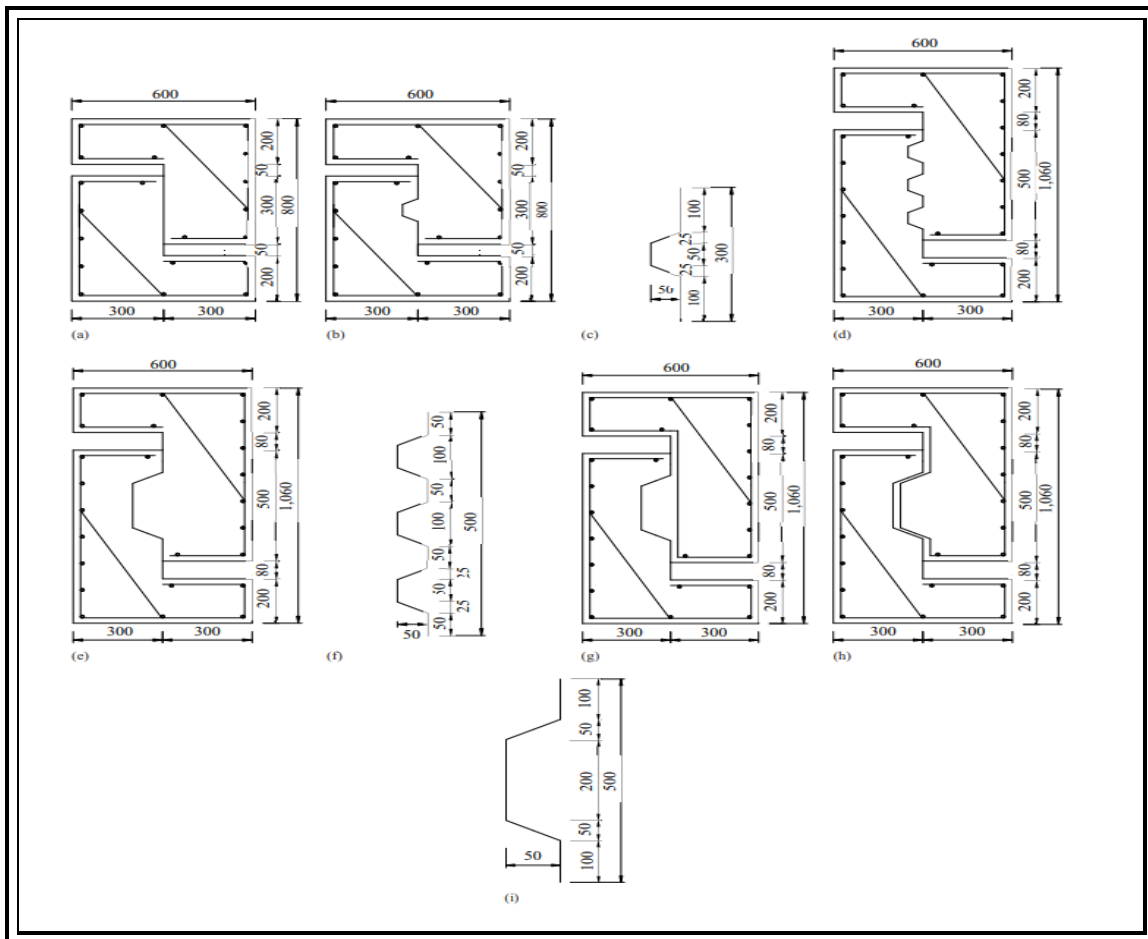
Figure 2- 2. Specimen dimensions and configurations for test specimens (in millimeters): (a) flat joint; (b) single-keyed joint; (c) detail of a single key in the shear region; (d) three-keyed joint; (e) large-keyed joint; (f) detail of three keys in the shear region; (g) large-keyed joints with straight reinforced bars; (h) large-keyed joint with key-shaped reinforced bars; and (i) detail of a large key in the shear region.(Liu et al., 2019).

Li et al. (2019) look into the direct shear characteristics of ultra-high performance concrete (UHPC), 15 monolithic placement specimens (MPSs) and 12 water jet prepared samples (WJTSs) were evaluated. Figure (2.3) depicts the direct shear test specimen.
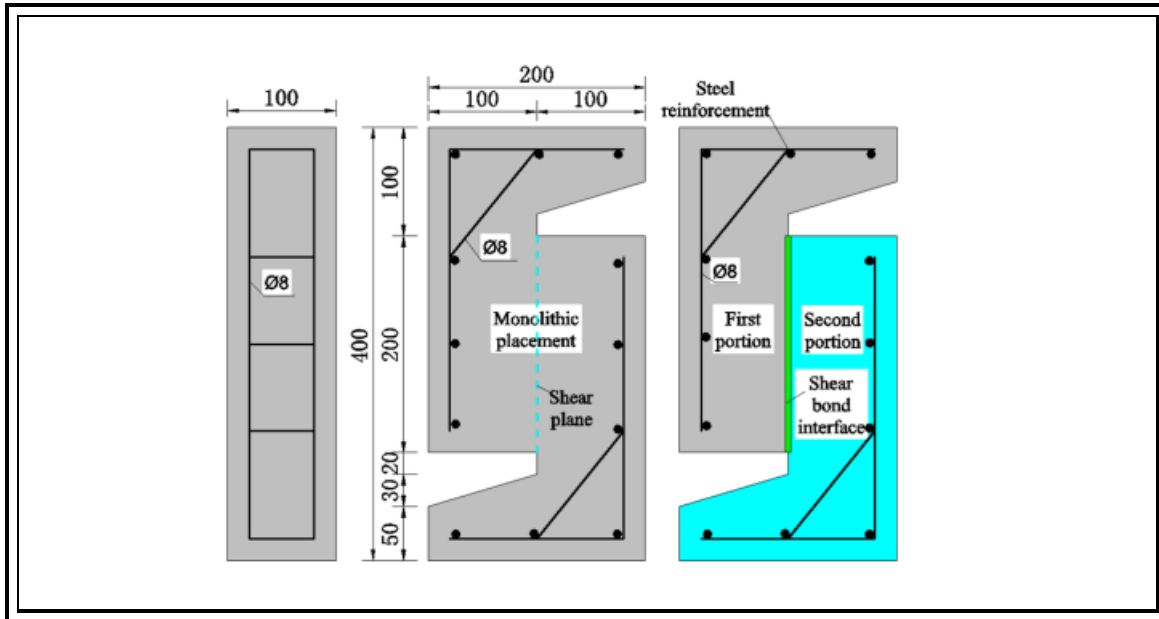
Figure 2- 3. Direct shear test specimen(Li et al., 2019).

Steel fiber shape, volume fraction, and interface treatment were all studied to see how they affected UHPC's direct shear properties. There was evidence of ductile failure in the MPSs, which were reinforced with steel fibers according to the test results. There is an increase in shear strength of 24.72 MPa when the fiber volume percentage increases. Steel fiber type has a little impact on shear strength and ductility; nonetheless, raising steel fiber length slightly decreases its shear strength. WJTSs made with 16 mm hooked-type steel fibers have a direct shear strength of up to 9.15 MPa, which is 2.47 times that of fiberless samples. The experimental results led to develop an interaction formula for the shear and compressive strengths, which predicted the cast-in-place UHPC constructions' shear load carrying capacity.

Gopal et al. (2020) investigated the shear behavior, shear capacity, and shear-transfer mechanisms of the ultra-high-performance fiber-reinforced concrete

14

(UHPFRC) keyed dry and epoxy joints. For this, a total of 12 full-scale shear joint key specimens were cast and experimentally tested until they failed. There were three variables that were used in the production and testing of keyed joint specimens: the number of shear keys, the confining stress, and the type of joint that was examined (dry or epoxy). Experiment results showed that the shear capacities of joint specimens increased by 150 percent when the number of keys increased, and by considering the effect of the epoxy layer, the keyed epoxy joints tended to produce higher shear failure capacities by 25 percent than the specimens with dry joints at higher confining stresses.

Jiang et al. (2021) evaluated the shear-friction of grooved construction joints between a precast UHPC girder and a cast-in-place concrete slab, 18 push-off tests were performed. Shear performance, the ultimate load upward slip relationship, and the shear capacity of the contact were studied, along with the impacts of slab type, shear reinforcement ratios, and interface treatments. It was shown experimentally that reinforcing the contact between joints significantly increased the ultimate shear resistance of a grooved UHPC substrate. The interface shear pressure is indeed affected by the cast-in-place slab variety. Surface modification of the grooved surface was shown to be an efficient method for boosting the shear capacity of an interface between a precast UHPC girder and a cast-in-place concrete slab. Furthermore, results obtained provided in this work well beyond confirmed a more precise formula found on the (Association Francaise du Genil Civil) AFGC 2013 guidance document that was developed to predict the interfacial shear strength between precast UHPC girders and cast-in-place concrete slabs. In theory, showed that the suggested formula might result in a joint design for bridges that is both more safe and more reliable.

Muzenski et al. (2022) used the findings of 11 contact shear experiments on monolithically cast UHPC and other tests from the literature to create a prediction model for UHPC. Experiments were performed using steel reinforcement at the contact with a range of yield stresses and reinforcement ratios to determine the shear capacity

of the interface. It was found, via the development of a prediction model, that the sum of the tensile resistances across the shear interface is an important factor in establishing the maximum shear strength. This contains the UHPC and reinforcement steel's tensile strengths. UHPC contact shear strength design recommendations are also given. The equation could be used to determine the contact shear capacity:

$$Vn = \left[\mu\left(A_{sv}f_s + A_{cv}\gamma f_{t,loc}\right) + A_{cv}c\right] < K.A_{cv} \qquad \text{2-1}$$

Feng et al. (2022) as a part of the push-off test, examine 65 Z-shaped ultrahigh-performance concrete (UHPC) specimens with monolithic and flat wet-joint surfaces (roughened with a high-pressure water jet). Keyed-joint shapes and confining stress are discussed in relation to the shear strength of UHPC specimens. Researchers suggest a high-precision equation to predict the shear capacity of specimens with monolithic interfaces, flat wet joints (WJs), and keyed-wet joints (KWJs). Steel fibers had a significant impact on increasing the shear strength of the UHPC specimens, according to the results of the tests. Shear strength rose approximately linearly with fiber content in the flat-wet-joint specimens. The shear strength was enhanced by using long, hooked-end fibers. Increasing the confining stress had no effect on the shear strength of the keyed-wet-joint specimens, which improved practically linearly with it. Increases in fiber volume fraction resulted in a decrease in strength reduction factor (the ratio of the ultimate shear strength to that of the monolithic interface) It is hypothesized that the fiber characteristic parameter has such an impact on the strength reduction factor.

2.3 Previous research on HSC shear friction

Kahn and Mitchell (2002) investigate the validity of the shear friction requirements in ACI 318 (1999)[17] for high-strength concrete. Fifty samples each of uncracked, fractured, and cold-joined push-off interfaces being examined. The contact surface was left as-cast in cold-joint specimens, creating a hard texture with an average amplitude of 6 mm, which is similar to an intentionally textured surface. Shear plane

diagonally cracking and widespread spalling in the concrete led to the collapse of cases with uncracked and cold-joint contact. Results showed no significant difference in the final strength between uncracked and cold-jointed samples. The following shear friction formula was devised for both uncracked and cold-joined rough surfaces, since the shear friction criteria in ACI 318[17] were deemed the most conservative in determining the interface shear strength for high-strength concrete:

$$v_u = 0.05f_C' + 1.4\rho_v fy \qquad\qquad 2\text{-}2$$

where the concrete's compressive strength fc ' was regulated at 20% of its maximum shear strength Vu(i.e., $vu \le 0.2fc\ '$).

In 2008 Mansur (2006) looks for a model that takes into account the effects of cracking to further assess the validity of models previously supplied by other researchers, and to find a more realistic model for precracked contact with high strength rated between 70 and 100 MPa. The 19 precracked push-off specimens utilized in this study had concrete strength and reinforcing parameter as variables in the experimental section. A total of 154 sets of data, including those from this study, were subjected to statistical analysis.

The strength of concretes was shown to be the most critical component in determining the contact cohesiveness. The true coefficient of friction of precracked surfaces was determined to be 0.55 and was found to be independent of the strength of the concrete. Only one version was suggested using the statement of (Walraven et al., 1987). This expression was given as:

$$\frac{v_u}{f_c'} = 0.566 \left(\frac{\rho_v fy}{f_c'}\right)^{0.5} \le 0.3 \qquad\qquad 2\text{-}3$$

The author also gave a quadtree relationship, whereby the shear transfer strength is calculated using an equation for each of the three linear segments of the idealized load-defamation curve. The normalized clamping stresses represent the initial fork ($\rho vf y/fc\ '$) less than 0.075, the proposed expression was:

$$\frac{v_u}{f_c'} = 2.5 \left(\frac{\rho_v f y}{f_c'} \right)$$
$$2\text{-}4$$

The ultimate shear transfer stress normalized to the concrete strength, based on the intermediate branch of the quadtree idealization, is provided by normalized clamping stresses ranging from 0.075 to 0.270:

$$\frac{v_u}{f_c'} = \frac{0.56}{(f_c')^{0.385}} + 0.55 \left(\frac{\rho_v f y}{f_c'} \right)$$
$$2\text{-}5$$

For larger amounts of normalized clamping stresses, permissible limits longitudinal shear transfer strength is denoted by the third straight branch. Author claimed that this restriction was necessary to ensure the steel's ductility when subjected to stress. Accordingly, the terminal linear branch is now defined as:

$$\frac{v_u}{f_c'} = 0.3$$
$$2\text{-}6$$

Single curve equation (2-6) was shown to produce more accurate estimates of shear transfer strength than the trilinear version, and was thus suggested for use in design.

Jiang et al. (2020) examined 12 different push off specimens. This study aims was to develop and estimate, using experimental data, a finite-element model of high-strength concrete single-keyed dry joints in PCSBs. Parametric research on repairing flaws in key, concrete strengths, and confining pressures was conducted based on that model. Among the quantitative findings were fracture patterns, load–slip relationships, and shear strength. The shear strength of single-keyed dry joints decreased when flaws were fixed, particularly on the bottom surface of the keys. This was due to an altered shear transfer mechanism. Shear strength enhanced by higher confining pressure and concrete strength. However, these factors either neutralized or exaggerated the impact of fixing flaws at the bottom surface of the key on shear strength, depending on which they were.

2.4 Previous research on NSC shear friction

Zhou et al. (2005) investigated the performance of precast concrete segmental box girder bridges at both serviceability and final strength using 37 push-off specimens. Gaining an understanding of joint behavior is crucial for predicting the bridge's reaction across its whole loading range. Plane and keyed, dry and epoxied, single-keyed and multiple-keyed full-scale joints with varying amounts of restricting stress and epoxy thicknesses were investigated in this research. Research has been conducted on the shear performance, shear capability, and shear transfer processes of these various joints. Finding that joints shear capacity improved with increasing confining stress and that epoxied joints continuously had better shear strength than dry joints despite the failure being more brittle than dry joints. As a result of improper key fitting, it was observed that the average shear strength for a key in multiple-keyed dry joints was lower than those in single-keyed dry joints. Epoxy reduced the effects of the fixing flaws and allowed the shear stress to be distributed evenly, thus the shear strength of keys in multiple-keyed epoxied joints was comparable to that of single-keyed joints. The AASHTO and other design standards were used to evaluate the experimental outcomes of these tests. These equations were shown to consistently overestimate the shear capacity of dry multiple-keyed joints by a large margin, while consistently underestimating the shear strength of single-keyed and multiple-keyed epoxied joints by values up to 40%. Therefore, the findings suggest that when applied to multiple-keyed dry joints, certain strength reduction variables must be incorporated to the design equations.

Harries et al. (2012) concerned with improving the understanding of how reinforced concrete-to-concrete contact behave in the context of the shear friction hypothesis. The major objective of this study was to provide experimental evidence for the assumption underlying all existing shear friction formulas, namely, that the shear strength is attained at the point where the steel yields diagonally to the shear plane.

There were 8 different push-off tests conducted, all under cold-joint conditions at the contacts. Medium strength steel with an average yield strength of 424 MPa and high strength steel with an average yield strength of 896 MPa were both utilized. In all cases, No. 3 (9.5 mm) and No. 4 (12.7 mm) bars were utilized as the standard sizes. According to the authors' findings, the final shear transfer strength was unaffected by steel grade. The main takeaway from this research is that even at the utmost load, stresses in the interface steel reinforcement remain far below the yield point. These results led to the suggestion that modulus of elasticity of steels, Es, rather than its yield strength, fy, should be utilized to establish clamping stresses at the ultimate load. The maximum shear transfer stress was expressed in three distinct ways:

For solid monolithic interfaces.

$$v_u = 0.075 \grave{f} c + 0.002 E_s \rho_v \qquad\qquad\qquad 2\text{-}7$$

For coarse cold-jointed contact.

$$v_u = 0.040 \grave{f} c + 0.002 E_s \rho_v \qquad\qquad\qquad 2\text{-}8$$

For cracked contact.

$$v_u = 0.002 E_s \rho_v \qquad\qquad\qquad 2\text{-}9$$

The friction coefficient was set to one, as implied by these equations. The author hypothesized that shear strength enhanced by external clamping forces before interface breaking. This indicates that they should be excluded from shear friction estimates if cracking along the contact plane is permitted. Vu is equal to 0.2fc ', which is the maximum possible ultimate shear transfer stress.

2.5   Previous research on hybrid UHPC/HSC and UHPC/NSC shear friction

Crane (2010) conducted an investigational study to calculate the shear capability of a ultra high performance concrete and high performance concrete interface, simulating the joining between UHPC girders and a HPC deck. The 19 precracked push-off specimens utilized in this study had concrete strength and reinforcing

parameter as variables in the experimental section. A total of 154 sets of data, including those from this study, were subjected to statistical analysis. 36 push-off experiments were conducted to determine the contact shear capability of precast UHPC and cast-in-place HPC. Contact plane preparation and interface reinforcement ratio were the key independent factors. The UHPC/HPC contact was analyzed using three distinct surface treatments. The initial interaction used a form liner 6 mm deep to imitate the fluted pattern of a typical raking surface on top of a prestressed girder, resulting in UHPC. As a second contact, the cast UHPC was given a somewhat hard texture using burlap. The third and final surface was the as-cast, smooth cold joint surface. Zero, one, two, or three two-legged No. 3 stirrups across the interface produced reinforcement ratios of 0%, 0.25%, 0.50%, and 0.750%, respectively, for shear reinforcement. Half of the composite push-off test specimens were cast from the same ultra-high performance component. After this half had cured, the other half was cast with HPC against the cold joint. The HPC and UHPC compressive strengths were measured to be 84.4 MPa and 200 MPa, respectively. The interface shear plane for all samples was a rectangle with dimensions of 174 millimeters in width and 288 millimeters in length. All of the push-off specimens were put through their paces under a constant load, as shown in Figure 10a. On both sides of the specimen, at the interface's center, the relative slip movement was measured. Overall, UHPC/HPC specimens without interface shear reinforcement failed suddenly at substantially lower stresses than those with reinforcement. The HPC shear keys at the interface of the fluted UHPC caused the shear failure see Figure 2-4.
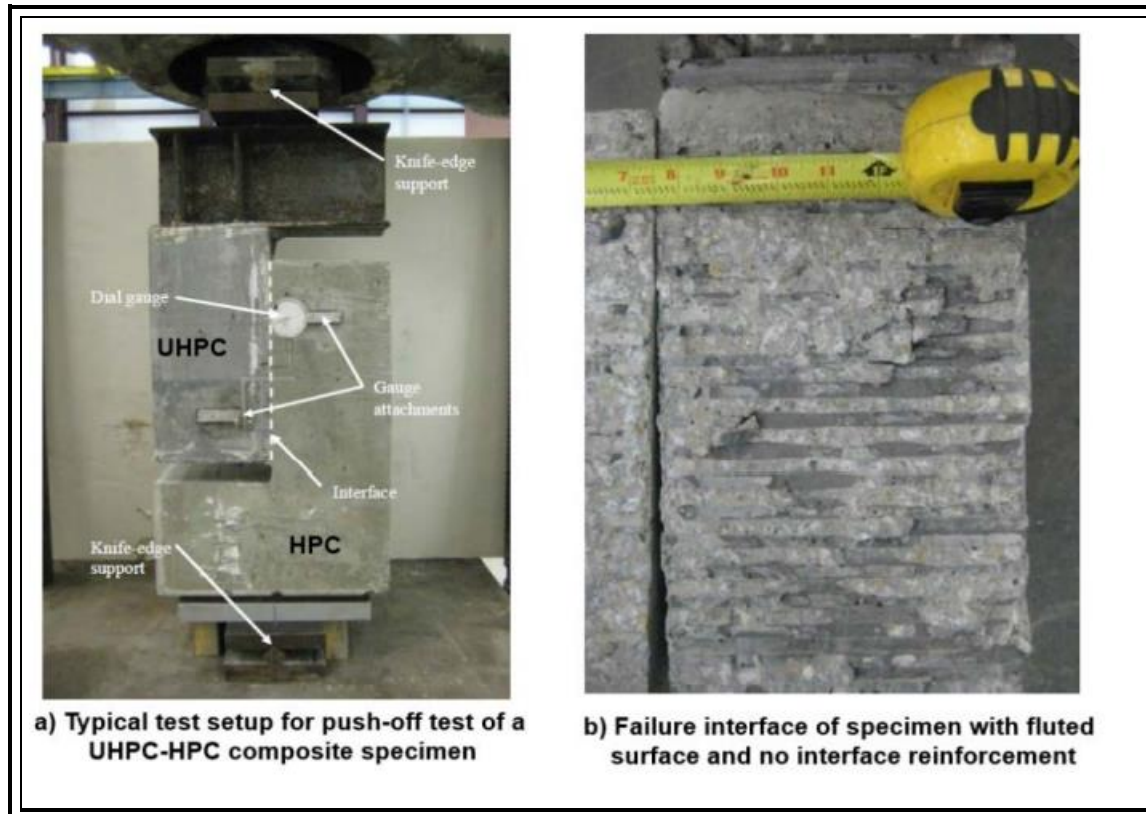
Figure 2- 4. Push-off specimen (Crane, 2010).

The following inferences were made in findings of the push-off tests and compared to the mathematical formulas in the ACI and AASHTO design codes:

- ➢ Compared to a smooth cold joint, the interface shear capacity enhanced by 127% when the surface was roughened with burlap, and by 228% when flutes were added.
- ➢ Once a flat contact is employed between UHPC and HPC, the shear strength rises linearly with the increase in the interface reinforcement ratio, verifying the validity of the shear friction hypothesis.
- ➢ The contact shear capability of composite UHPC/HPC structures cannot be accurately estimated using the current regulations of the American Concrete Institute and the American Society of Highway Engineers.

In 2017 Jang et al. (2017) examined 12 push-off specimens that are divided into two sets. The push-off test is used in this study to evaluate the shear strength and failure mechanism of plain UHPC construction joints. Five interface treatments (water jet (WJ), vertical joint (VJ), grooved joint (GR) with individual sizes of 10, 20, and 30 mm) and the monolithic reference case (MN) are shown in figure (2-5). The combined set of UHPC (180 MPa) and the set of NSC (30 MPa) and UHPC are both considered for placement (180 MPa).
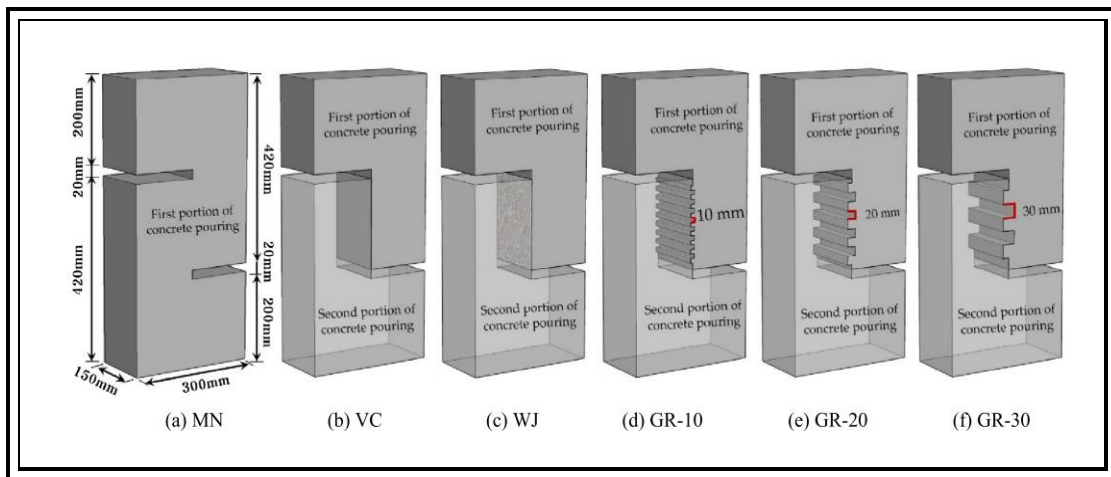
Figure 2- 5. Configuration of specimens(Jang et al., 2017).

The shear behaivior of construction joints combined with NSC and UHPC may be greatly enhanced by using a sample with a water jet joint. This finding provided conclusive evidence for the significance of the coarse aggregate interlocking mechanism present in typical concrete. Thus, evenly distributed interfaces at the water jet-formed joint can avoid much stress concentration compared to affectedly formed interfaces formed by box-shaped grooves. Construction joints with at least 20 mm grooves improve the shear performance of construction joints significantly for the combined set of UHPC. Shear strength is increased 1.78 times and 2.45 times for 20 mm and 30 mm grooves, respectively, when compared to water jet. This result indicated that for UHPC construction joints, careful measures other than the water jet used in ordinary concrete construction joints are required.

23

Liu et al. (2020) tested 16 push off specimen to understand the shear bond performance of the interfaces between UHPC and NSC. Different forms of interfaces evaluated the shear bond performance of 16 push-off specimens at UHPC/NSC contacts. Different forms of interfaces between UHPC and NSC, such as bubble groove interfaces, flat-surface interfaces, and water-jet-surface interfaces, were experimentally examined in this study, as shown in Figure (2-6).

Evaluation parameters included contact forms, the presence of dowel rebar, and the order in which UHPC and NSC were formed. The series of bubble groove interfaces also included research and testing on 3 distinct sized bubble grooves. Push-off experiment data was analyzed for connections among loads and slip, strength characteristics, and types of fracture. The bulk of the jointed samples collapse as a consequence of NSC degradation, and the test findings demonstrate that the ultimate stress of the jointed samples is less than that of the monolithic reference specimens. Therefore, the NSC plays a crucial role in establishing the shear performance of the UHPC-NSC interfaces. Distinct molding phases of UHPC and NSC greatly impact the shearing strength of varied contacts between UHPC and NSC, leading to different
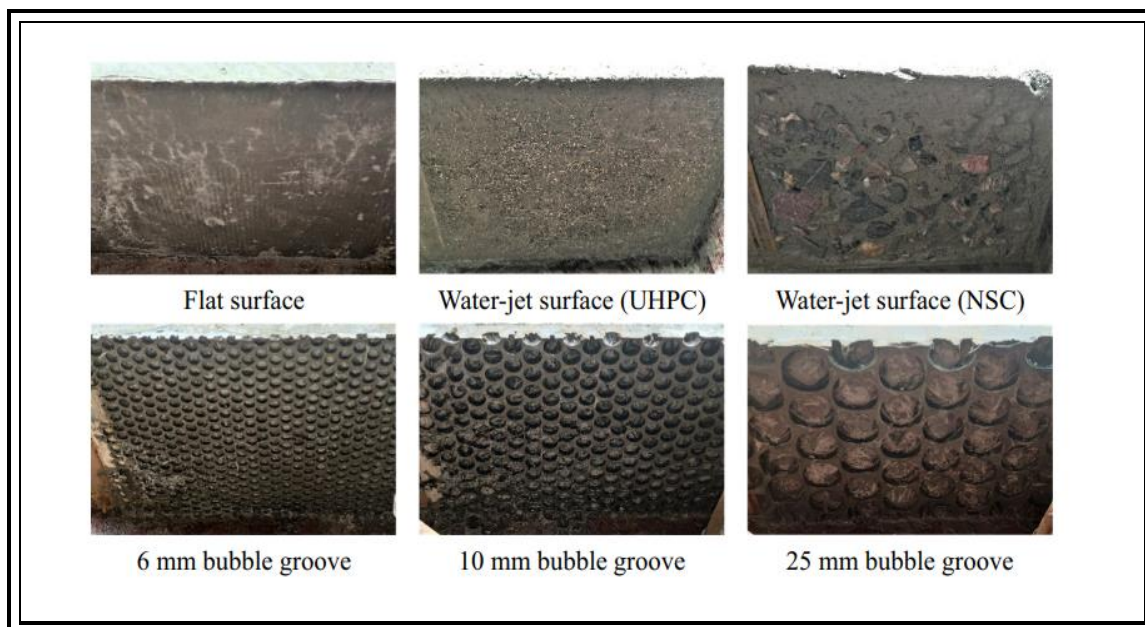
Figure 2- 6. Shapes of different joints(Liu et al., 2019).

failure modes of the specimens. Both the water-jet and the bubble-groove interface, both 10 mm in width, are eligible for use in making the connection between an NSC substrate and UHPC overlay. Shearing damage occurs at the bottom of the embossments on the NSC overlay at bubble groove contacts between the UHPC base and NSC top, whereas the water-jet interface has rather poor shear performance. Specifically, shearing damage occurs at the bottom of the embossments on the NSC overlay, where the bubble grooves of the UHPC substrate meet the overlay.

Semendary et al. (2020) studied, the interface bond performance between precast high-strength concrete (HSC) and cast in situ (UHPC) was investigated utilizing the push-off test under direct shear. Prior to and during contact collapse, the impact of shear reinforcement on load transmission was analyzed. This experiment's results were also compared to benchmarks established by regulatory requirements. The results of the adhesion tests demonstrated that UHPC outperforms prefabricated concrete in this regard, with an adhesion value that is higher than the monolithic surface adhesion value required by the standards. Data analysis suggests a bond strength versus slip model that could be used to forecast the HSC-UHPC interface when subjected to shear stress. Important in reducing contact slide before to collapse was shear reinforcement placed across the contact. The socially defined code designing with a high shear capacity is a safe bet. Once the ultimate force was achieved, the load-slip relationship dropped, indicating that the adhesion strength had already been attained. As the maximum stress of UHPC cast versus HSC was higher than that of the past studies, the shear maximum stress of $0.618f'c$ could be utilized to estimate the contact adhesion bond strength under direct shear. Here, $f'c$ denotes the lower concrete compressive strength at the interface in MPa. This study's shear capacity was also higher than the AASHTO LRFD 2016 ACI318-14 and 2010 CEB-FIB Code requirements for specimens with SR throughout the interface. Therefore, it seems that all programs represent very cautious implementations of HSC-UHPC connections.

Farouk et al. (2022) employed a mathematical model, to research the shear strength of the UHPC/NSC contact. Study results were used to develop a shear strength model for a long-span, UHPC-NSC hybrid girder with a groove interface. The UHPC-NSC connections were studied using a finite element model. The actual data obtained from the push-of test corroborated the results of a computational study of the interface shear performance of precast NSC and cast-in-place UHPC with different interfaces, including the box groove. The numerical solution yielded reliable findings. The findings of the simulated analysis suggested that the ultimate shear resistance of the interface established with the groove surface may be greatly improved by reinforcing it across the UHPC-NSC contact. Because of the eccentric loading distance, the final shear resistance was somewhat less. With regards to prediction, the AFGC-2013 rules outperform both the ACI 318-14 and the AASHTO LRFD.

2.6 Summary

Due to its design fragility, concrete-to-concrete connects have been properly and regularly studied throughout time, particularly those between precast girders and cast-in-place slabs. This section provides a synopsis of the preceding studies undertaken by other specialists. Different design statements and assumptions were used to explain the behavior of contact surfaces under direct shear stresses. The importance of shear transfer design criteria in major codes was stressed and examined in depth. Previous research could be summed up as follows:

➢ The majority of the design expressions presented in the preceding study were generated from the analysis of push-off specimen test results. (Anderson, 1960, Hanson, 1960)introduced these specimens, which were reported to behave similarly to the interfaces in composite concrete beams. It was found that the shear transfer mechanism among concrete layers is a multifaceted issue that depends on a wide range of factors, such as the contact coarseness, the concrete's

compressive strength, the stresses produced by perpendicular forces at the interface, and the amount of reinforcement crossing the interface. Due to the complexity of the problem, it is not possible to explicitly separate all of the elements that influence shear transfer behavior or to develop explicit analytical correlations between these parameters.

➢ In a major improvement over prior techniques, steel reinforcement is now being used exclusively in the production and study of concrete-to-concrete contacts. As a result, the purpose of this study is to evaluate several types of interfaces for annotative applications.

➢ The shear friction concept has been embraced by the majority of researchers and design codes throughout the globe, despite the fact that several shear transfer models have been developed to account for various conditions of concrete surfaces (such as cracked, uncracked, and cold-joint). The most developed version of this theory postulates that 3 separate processes contribute to the transmission of shear over the concrete-concrete interface: 1) cohesion; 2) friction; and 3) the action of dowels. Several design ideas given by different scholars since 1960 were also uncovered by the literature review. These formulations were useful in a wide variety of contexts, including monolithic concrete interfaces, concrete masonry component interactions with rough, intermediate, or smooth contact surfaces, and precast concrete interfaces.

It is well known from the literature mentioned above there is lack in knowledge about the shear friction of UHPC in the local reasearch.

Chapter Three: **Research Methodology**

3.1 Introduction

The testing program of the present research program involved casting and testing nine push-off test specimens to fully investigate the behaviour of concrete joints with UHPC utilized as shear transfer reinforcement.. summary of the experimental program, including resources, examined samples, design and production specifications, information about the surfaces studied, and test equipment. Primary components such as force applied, slide, and contact pressures at peak load are used to show test findings. The next parts include a summary of the test findings and an analysis of the test datas.

3.2 Details of The Test Specimens

3.2.1 General Description

All the specimens used in the experiments were designed to be pushed off. As can be seen in Figure 3-1, the testing sample comprises of two L-shaped concrete blocks. The shearing surface measures is 240 mm in width, 490 mm in length, and 120 mm in thickness; it is a component of the L-shaped web. The major role of the flange is to make available a concentric shear force in the shear surface between the two components. To assure pure shear behavior, a 20 mm gap was placed between the connected sections. Standard measurements for the push-off specimen are shown in Figure 3-2. Nine distinct push-off specimens were produced and examined using UHPC with varying contacts.

3.2.2 Designation of specimens

A symbol for each push-off specimen has been set to distinguish it from the rest of the specimens which includes (type of interface). as listed in Table (3-1).

Figure 3- 1. Push-off specimen.
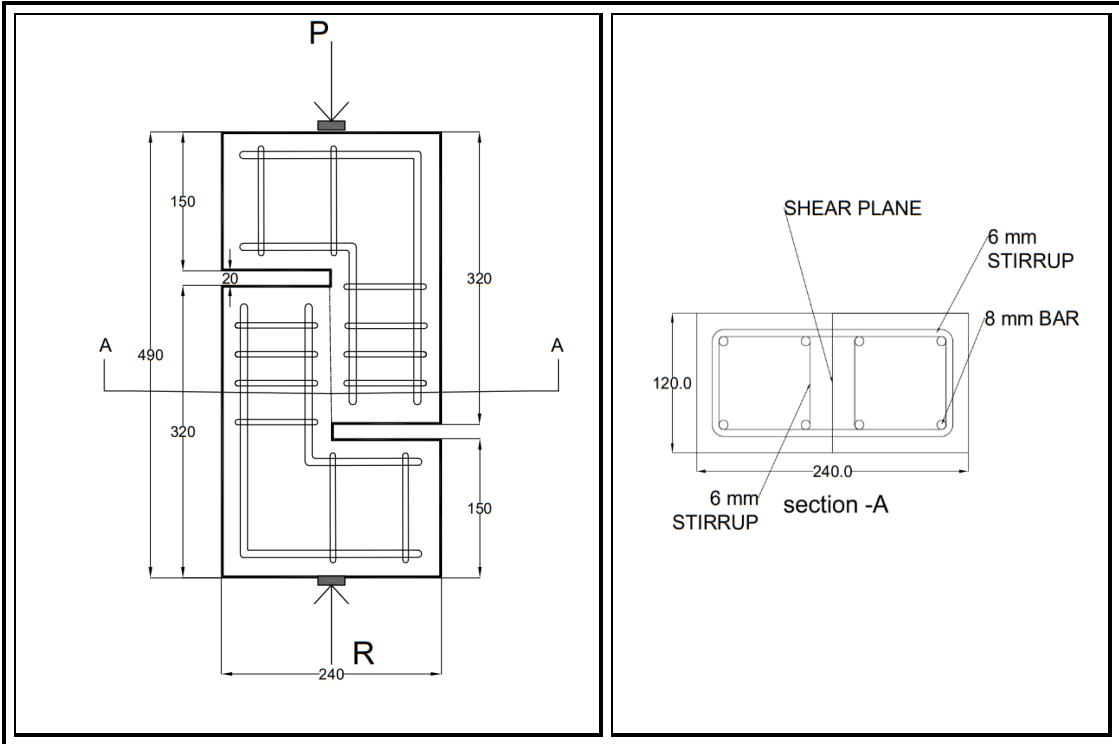
Figure 3- 2. Dimensions of the specimen in (mm).

Table 3-1.Details of the tested specimens.

No	Type of interface	Specimens ID	fc' (MPa)	Av (mm2)	ρv (%)
1	Control	CS	120 MPa	120*150	N
2	Rectangular grooves	RGS	120 MPa	120*150	N
3	Circular grooves	CGS	120 MPa	120*150	N
4	Triangular grooves	TGS-25	120 MPa	120*150	N
5	Triangular grooves	TGS-35	120 MPa	120*150	N
6	Exposed fiber	EXFS-1	120 MPa	120*150	N
7	Exposed fiber	EXFS-2	120 MPa	120*150	N
8	Dowel bar	DBS-1	120 MPa	120*150	0.31%
9	Dowel bar	DBS-3	120 MPa	120*150	0.94%

3.2.3 Description of Test Specimens

One of these specimens is monolithic specimen as a control specimen to compare the behavior with other specimens. All specimens had the same dimension. All specimens had a similar clear cover of 20 mm from each exterior concrete face to the longitudinal reinforcement. The shear plane is similar for all specimens(150*120mm). As shown in Figures (3-3) to (3-5), details of reinforcement included (4ø8mm) diameter

of deformed bars were provided as longitudinal reinforcement and (4ø6mm) stirrups in order to ensure shear failure to occur rather than flexure failure.
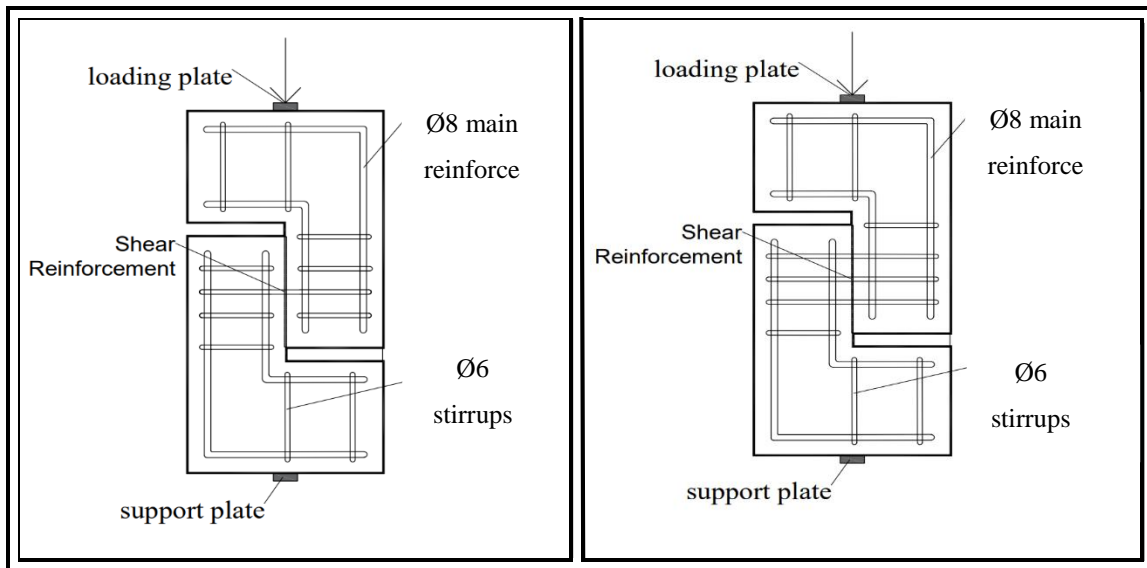
Figure 3- 3 Geometric and reinforcement details for Dowel bar specimen.
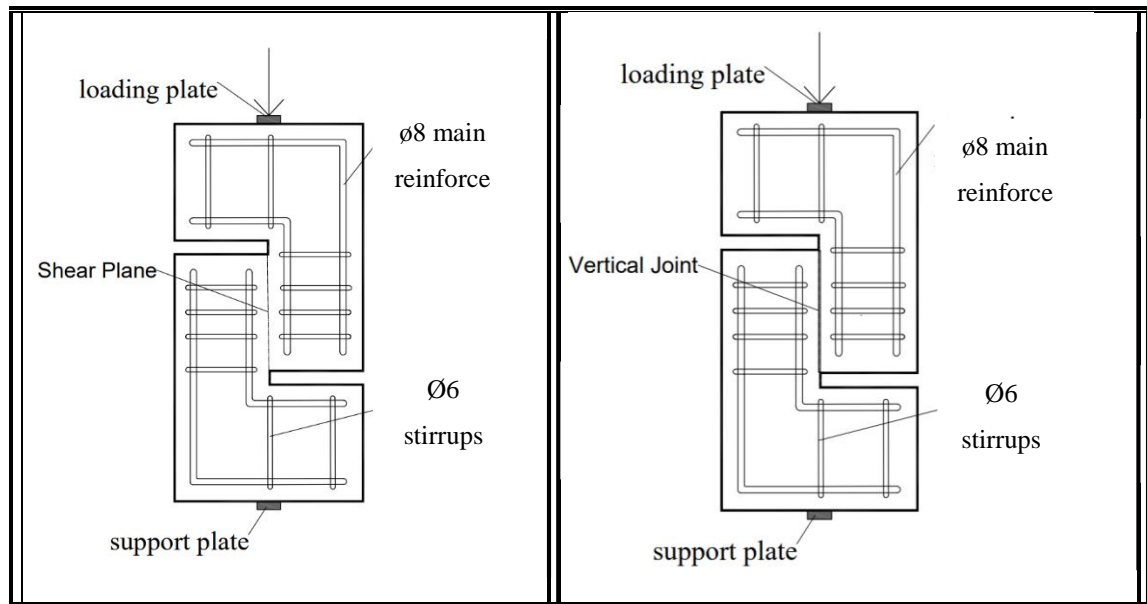
Figure 3- 4 Geometric and reinforcement details for Control and EXF specimen.
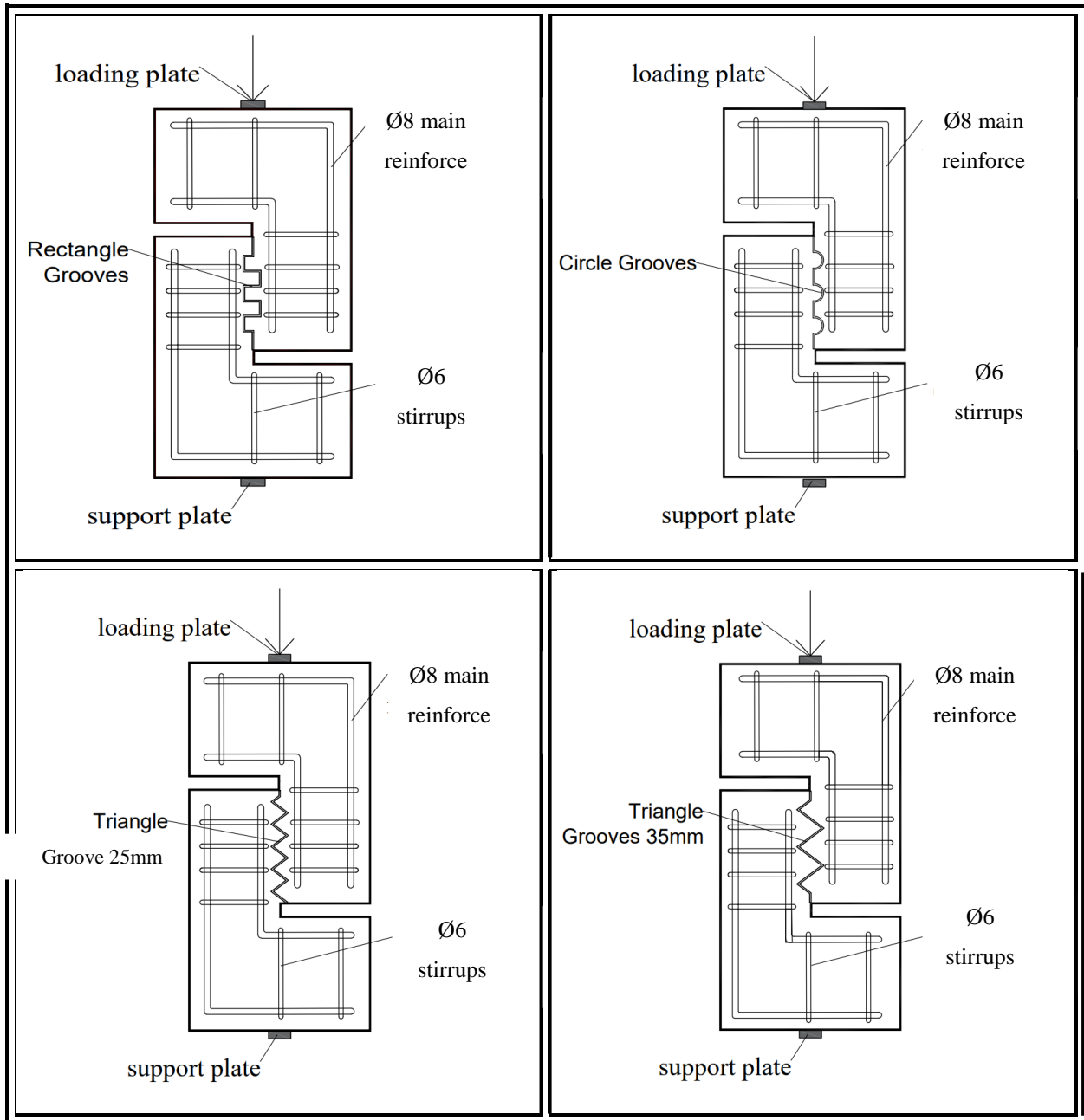
Figure 3- 5. Geometric and reinforcement details for grooved specimen.

3.2.4 Fabrication of Test Specimens

Plywood strips utilized as the molds to help achieve the desired push-off specimen shape as shown in Figure(3-6). The grooves and overall form of the exquisite specimen are produced using a computer numerically controlled machine. Every sample was cast in two phases to obtain the cold-joint state. For the initial part of the

specimen, the web of the L-shaped block was laid flat during casting. To avoid flexural fractures in the L-web shapes and flange during testing, steel bars and stirrups were added in both the longitudinal and transverse directions as shown in Figure(3-7). The concrete had a good vibration once it was placed. To generate a naturally compacted coarse contact, the top surface was additionally vibrated as shown in Figure 3.8. The first part of the specimen was cast and left in the formwork for 24 hours and then placed in the curing for 28 days, after 28 days of curing the second part was cast and left another 28 curing days. The specimens were additionally sprayed with white paint to ensure that any cracks that appeared during the test could be easily seen.

Figure 3- 6. Playood form work.
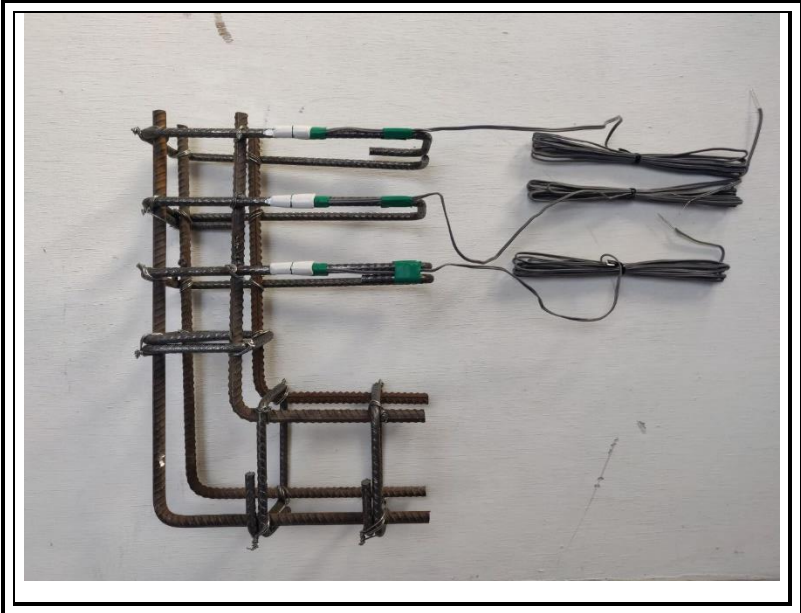
Figure 3- 7. Reinforcement cage.

Figure 3- 8. The casting process.

35

3.3 Materials Properties

3.3.1 Cement

Ordinary Portland cement (Iraqi manufactured) named al-jesar was used throughout this investigation for casting all the specimens (UHPC). Its chemical composition and physical properties supplied by the manufacturer are given in Table (3-3), respectively, which conforms to the Iraqi standard specification No. 5-1984(5, 1984).

Table 3-2. Chemical analysis and main compounds of cement.

Composition of oxides	Abbreviation	%By weight	Limits of IQS No. 5/1984
Lime	CaO	53	-
Silica	SiO_3	20	-
Aluminum	Al_2O_3	3.8	-
Iron oxide	Fe_2O_3	5.2	-
Sulfate	SO_3	2.2	$\leq 2.8\%$
Magnesia	MgO	3.6	$\leq 5\%$
Loss on ignition	L.O.I	3.2	$\leq 4\%$
Lime saturation factor	L.S.F	0.86	0.66-1.02

Insoluble residue	I.R	0.68	≤1.5
Main compounds (Bouge's)	%By weight of cement		
Tricalcium silicate(C3S)	48.04	-	
Diacalcium silicate(C2S)	22.5	-	
Tricalcium aluminate(C3A)	1.55	≤3.5%	
Tetra calcium alumino ferrite(C4AF)	16.74	-	

3.3.2 Fine Aggregate

Natural fine aggregate imparted from the region of (Kerbala) was used as natural sand in UHPC. This natural sand was too fine to be used successfully in making mortar. sand that was sieved by (300 μm sieve). Table (3-4) shows the physical and chemical characteristics of fine aggregate. It conforms to the (IQ. S No.45/1984) (45, 1984) limitation zone (4).

Table 3-3.Fine aggregate physical and chemical properties.

Physical and chemical properties of fine aggregate.		
Property	Test Results	Limits of IQS No. 45/1984
Specific gravity(kg/m^3)	2.60	-
Fineness modulus	1.45	-
Sulfate content SO3(%)	0.38%	$\leq (0.5)$

3.3.3 Silica Fume

MasterRoc MS610 the grey densified silica fume utilized in the combination is sourced from BASF Chemical Company. The particles of silica fume are hundreds of times smaller than cement particles, hence it is only ever used as a partial substitute for cement or as an addition to enhance the qualities of concrete. The data from the silica fume testing for this investigation are shown in Table (3-5), and it conforms to the chemical ASTM C1240-20(ASTM, 2020).

Table 3-4. Results of silica fume tests.

Form	Powder
Color	Grey
Density kg/l	0.55-0.7
Chloride content	<0.1%

3.3.4 Steel Fiber

This study used commercially available micro steel fibers to create UHPC. Steel fibers of this kind were manufactured by a Chinese firm based in Jiangxi Province (Mainland). The current investigation makes use of it with the aspect ratio (Lf/Df)= 65 and volume fraction (Vf =2%). Fiber steel characteristics are shown in Table (3-6).

Table 3-5. Properties of the steel fibers tests.

Property	Specifications
Type	WSF0213
Surface	Brass coated
Form	Straight
Density (kg/m³)	7860
Melting Point (°C)	1500
Length (mm)	13
Diameter (mm)	0.2
Aspect Ratio	65
Tensile Strength (MPa)	Minimum 2300
Modulus of Elasticity (GPa)	203

3.3.5 Mixing Water

All the samples were cast and cured using regular tap water.

3.3.6 Chemical Admixture

"Master Glenium 54," a Super plasticizer manufactured by the BASF Company in Germany, was employed throughout this investigation for UHPC. This material has been classified as type (F) and (G) in ASTM C494- 13(ASTM, 2013). The technical properties of Super plasticizer are presented in Table (3-7).

Table 3-6.Technical description of master glenium54.

Properties	Master Glenium 54
Consistency	Turbid liquid
Color	Light green
Density (g/cm^3)	1.07
PH	5-8

3.3.7 Steel Reinforcement

Deformed reinforcing steel bars (Ukrainian source) were employed in this work with diameter (ø8mm) as longitudinal reinforcements, for all tested push-off specimens. In addition, deformed steel bars (ø6mm) were used as closed horizontal and vertical stirrups as shown in Figure(3-9).

Figure 3- 9. Reinforcement test.

3.3.8 Concrete

Concrete with 120 MPa were used. Concrete was prepared at the casting bay and then poured, fine aggregate consisted of sand sourced from the area. Each of these components was locally supplied. Table 3.2 displays the mixing ratios required to produce a material with a certain strength (120 MPa) . Each concrete patch required at least six cylindrical molds measuring 150 mm by 75 mm. These cylinders were treated in the same way as their respective test specimens. Cylinders examined during the same day as their equivalent samples had average compressive strengths of 120 MPa for both the first and second L-shapes. In according to ASTM C39-12 (ASTM, 2012) and ASTM C496-11 (ASTM, 2011), respectively The compressive strength fc' and the splitting tensile strength ft of the concrete were measured.

Table 3-7.Details of mix proportions in Kg for m³.

Cement	Silica fume	Fine aggregate	W/B	Superplasticizer	Steel fiber
950	190	1050	171	34.2	157

3.4 UHPC Mix Design

3.4.1 Mix Proportion of UHPC

UHPC (with steel fibers 2%) were used for all push-off specimen. During the early stage of the current study, many trial mixes were performed and tested at age of 7 days. The selected mixture ratios were sufficient to give an adequate compressive strength about (120) MPa at 28 days and a suitable workability.

3.4.2 Mixing Procedure of UHPC

For UHPC, the cement, fine sand, and silica fume were mixed in dry case for about 5 minutes to dissipate the fine sand particles throughout the cement particles and silica fume. The admixture was dissolved in water and added gradually during the mixing process; the mixture was then stirred for four minutes. Steel fibers were uniformly distributed into the mix. In all, from the time water is added to the mix until the time the batch is ready for use, the mixing process takes around 20 minutes.

3.4.3 Curing of specimens

The curing methods adopted for this type of concrete cannot be compromised as this goes a long way in determining its applicability. Also, the physical, mechanical, and durability characteristics of UHPC can be greatly influenced by curing regimens used. Therefore, curing is a way or method of ensuring that the hydration process of the

cement is completed effectively by controlling the temperature in the concrete mix and maintain throughout the hydration process. Commonly employed curing regimes to achieve desirable mechanical properties for UHPC are: Standard Thermal Treatment, Delayed Thermal Treatment, Tempered Temperature Thermal Treatment, and Air Temperature cure (Graybeal, 2006). Standard thermal treatment or steam curing is when the specimens are cured at 60° C. In this study water with 60° C was used for curing of specimens for 28 days.

3.5 Concrete Tests

A number of tests were conducted to estimate the properties of UHPC in fresh and hardened states.

3.5.1 Mechanical Properties of Hardened Concrete

All samples were left for 48 hours in the mold. After that, they were removed from the molds and set in a basin full of clean water. Following 28 days, they were taken out of the container and tested with each push-off specimen at the same time according to the standard specifications ASTM- C39/C39M-12 and C496-11(ASTM, 2011) to obtain the compressive and splitting tensile strengths respectively, by using a universal testing machine with a capacity of 2000 kN.

3.5.1.1 Compressive Strength

ASTM C39/C39M-12 is the standard for measuring cylinder concrete's compressive strength (fc') (ASTM, 2012). At 28 days old, six cylinders (75 mm 150 mm) from each mixture were subjected to a digital compression testing equipment with a 2000 kN capacity see figure (3- 10).

Figure 3- 10. Compressive strength test.

3.5.1.2 Tensile Strength (f*t*)

The splitting tensile strength test was performed according to ASTM C496-11(ASTM, 2011). 75×150 mm cylindrical concrete specimens were used at ages of 28 days. Wooden bearing sheets of 3.0 mm thick, 150 mm wide, and 200 mm in length were attached to the top and bottom of the cylinder specimen, as illustrated in figure (3-11). A diametrically applied load with a capacity of 2000 kN was applied down the length of the specimen until failure of the cylinder resulted, as indicated by the appearance of a transverse fracture that split the cylinder in two.

$$F_{st} = 2P/\pi ld \tag{3-1}$$

44

Where f*st* is splitting tensile strength in (MPa), P is the applied compressive load in (N), D is the diameter of cylinder in (mm), and L is the length of cylinder in (mm).
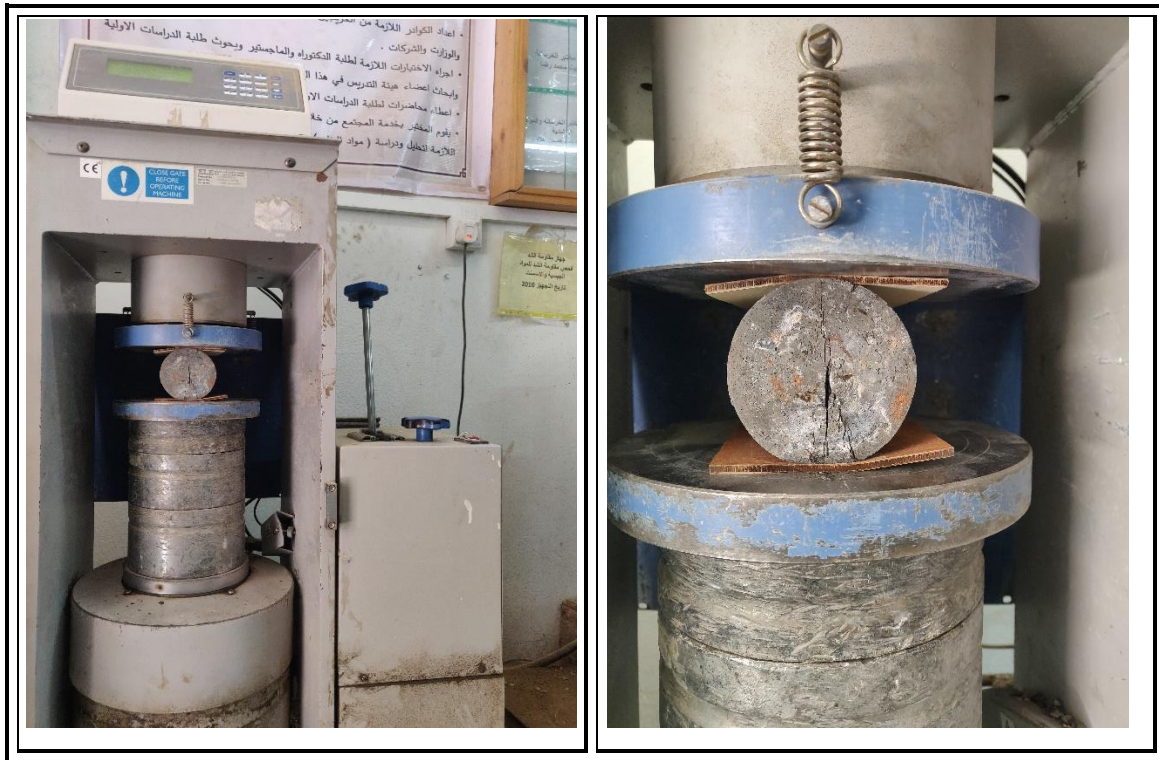
Figure 3- 11. The splitting tensile.

3.6 Instrumentations

A linear variable differential transducer were taken beside the load cell to track the applied shear force.

3.6.1 Measurement of Slip

For each sample, the amount of relative slip between the push-off specimen's two halves was measured along the shear plane. The push-off sample was equipped with a linear variable differential transducer (LVDT) in both the horizontal and vertical planes. One end of the LVDT was secured to one portion of the specimen, while the other, legal end was supported by an aluminum bracket connected to another region of the same specimen. The measured slips were captured by connecting the LVDTs to a data gathering device.

3.7 Test Setup and Procedure

Once the samples had cured, they were painted white so that any cracks could be easily seen. After that, the specimens were placed vertically on a lower, sturdy steel support and placed under the examination frames hydraulic jack. A uniform force was applied to the sample in a direction perpendicular to the shear plane. Figure 3.12 and Figure 3-13 shows a diagram of the test apparatus and the instruments that were made available. With no bending moment, this loading situation merely produced direct shear onto the shear plane. In order to test the samples strength, they were loaded uniformly at a rate of 20 kN per minute. When the slip rose significantly in response to a sudden decrease in load, it was deemed to have failed. Load was paused at regular intervals so that fractures could be identified. Throughout the duration of the test, the qualitative performance of each sample was monitored. The concrete cylinders performance was evaluated on the same day as the reference specimen's performance.

Figure 3- 12. The LVDT setup.
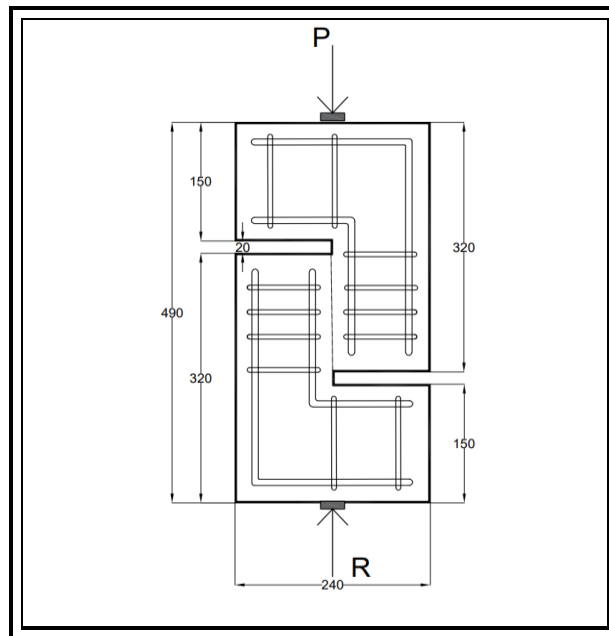
Figure 3-13. Typical specimen
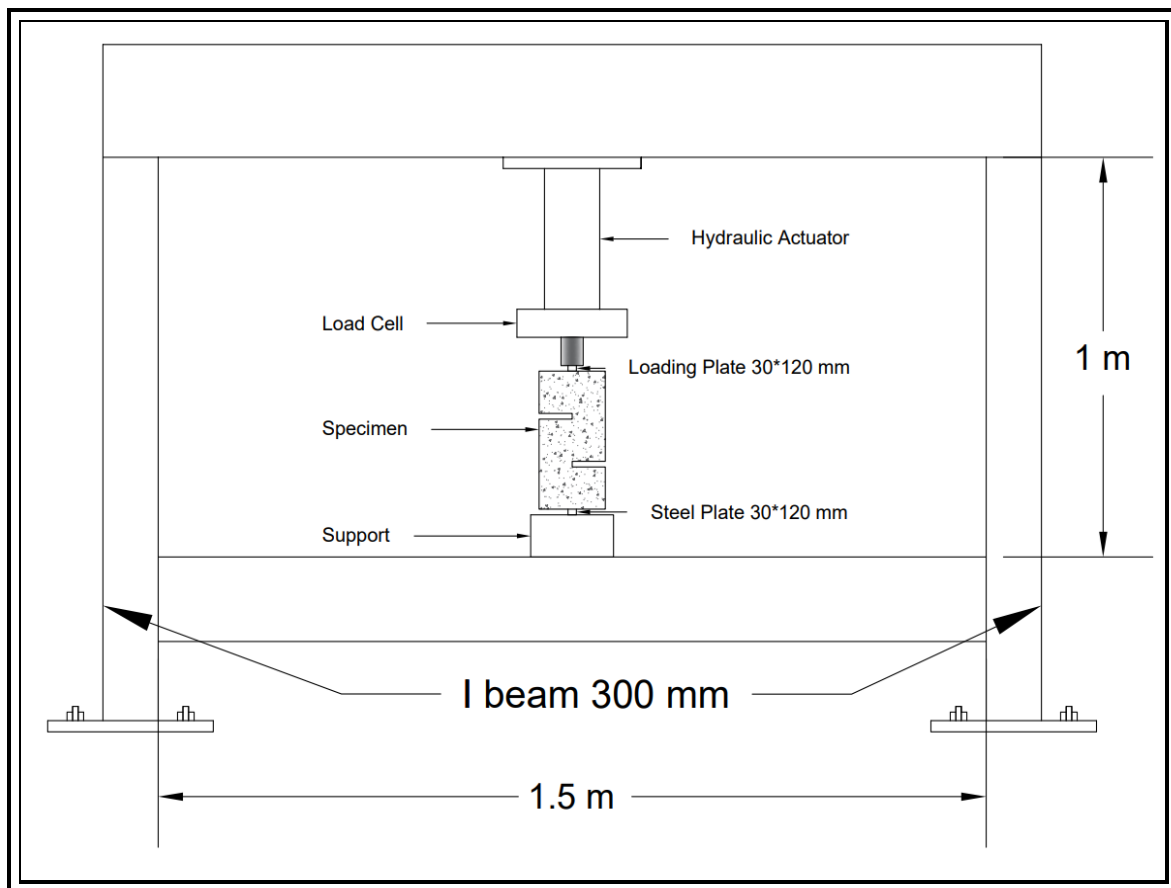
Figure 3- 14. Test setup front view.

47

Chapter Four: Experimental Results and Discussion

4.1 Introduction

This chapter provides a summary and discussion of the most important findings that were achieved from the experimental program outlined in the previous chapter. To begin, the results of the tests conducted on the control samples (cylinders), followed by the qualities of the concrete that were discovered. The load-slip response, ultimate strength, failure modes, stiffness criteria, and ductility index are among the test data acquired from push-off specimens that are then presented and analyzed.

4.2 Mechanical properties of concrete

Compressive strength, splitting tensile strength, and all other concrete examinations relating to fresh and hardened concrete qualities have been described and examined here. Casts of cylinders made from the concrete mixtures were analyzed for their characteristics.

4.2.1 Compressive Strength

Table (4-1) summarizes the findings of compressive strength tests conducted on the various mixtures at varying ages, and this section describes those findings. Six cylinders (150*75) mm were examined at ages of 7 and 28 days for each concrete mix, and the findings indicate the average strength value of these tests(ASTM, 2012).

Table 4-1.Compressive strength at different ages.

Compressive strength MPa		
Specimen ID	7 days	28 days
CS	95	123.2
RGS	92	120.5
CGS	92	120.5
TGS-25	90.5	122.1
TGS-35	90.5	122.1

DBS1	89	119
DBS3	89	119
EXFS1	95	121
EXFS2	95	121
Average	92	120.9
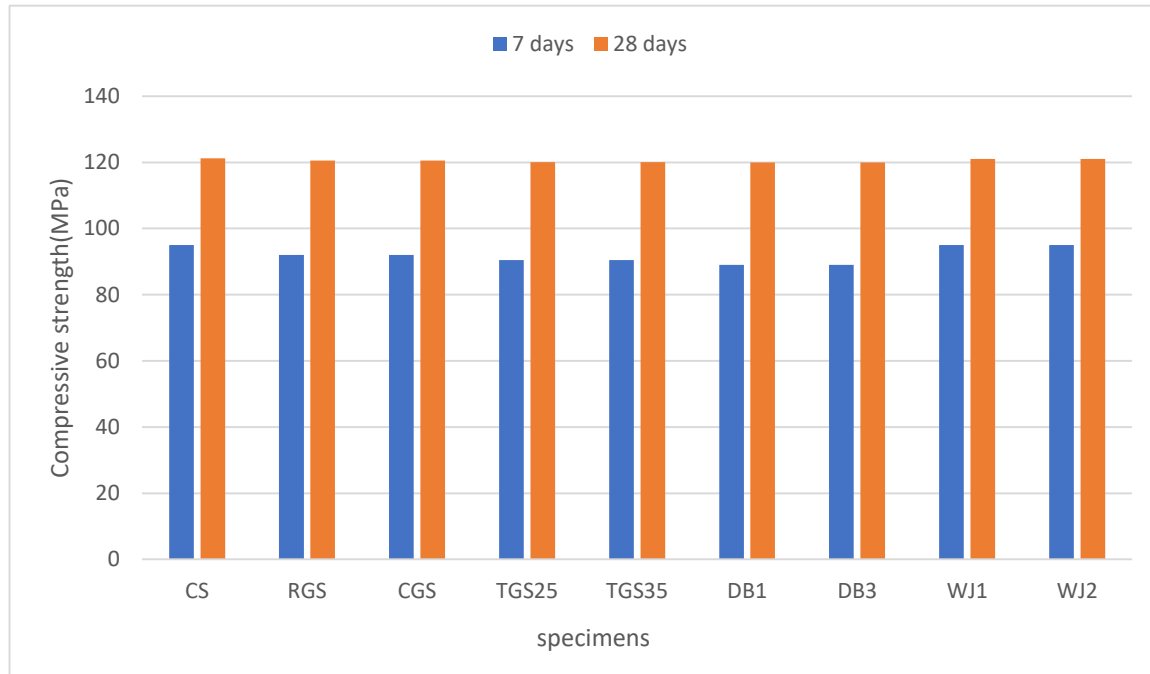
Figure 4- 1. Compressive strength at 7 and 28 days for each specimen.

4.2.2 Splitting Tensile Strength

Tensile strength at the point of fracture is a representation of the indirect tensile test technique. six cylinders (150*75) mm ASTM-C496(ASTM, 2011) utilized in each batch, with an averaged value representing tensile strength of concrete. Table (4.2) shows these values for UHPC at 7 and 28 days.

Table 4-2.Splitting tensile strength.

Splitting tensile strength MPa		
Specimen ID	7 (days)	28 (days)
CS	7.9	11.30
RGS	6.9	10.75
CGS	6.9	10.75
TGS25	7.35	11.10
TGS35	7.35	11.10
DB1	6.78	10.70
DB3	6.78	10.70
EXFS1	7.42	10.28
EXFS2	7.42	10.28
Average	7.20	10.77

4.3   General Behavior

Generally, the specimens are divided in three groups as following: the grooves specimens which include (rectangle grooves, circle grooves, and triangle grooves), dowel bars (DB1, and DB3), and exposed fiber (EXF1, and EXF2), in addition to the control specimen. All the three groups are discussed in term of load-slip, shear strength, failure mode, ductility index, and stiffness. All specimens were tested to investigate the influence of various interfacing techniques on their structural behavior relating to the control specimen.

Table 4-3. Result of the teasted specimens.

Specimen designation	Cracking load (KN)		Slip (mm)	Ultimate load (KN)
	Flexural crack	Shear crack		
CS	95	140	1.4	320
RGS	82	100	0..25	160
CGS	34	50	0.3	77
TRGS25	-	30	0.35	45
TRGS35	-	30	0.31	67
DBS1	-	20	0.55	46
DBS3	-	37	0.26	64
EXFS1	-	10	0.91	15.77

4.4   Load-slip response and cracking patterns

Generally, there are three stages of load-slip response: elastic uncracked, elastic-cracked and ultimate stages, where the first stage ended when cracks started, as shown in Figures (4-2) to (4-9). At the elastic un-cracked stage, the slip linearly increased in all specimens with loading, because the materials in the compression and tension zones were elastic. In elastic-cracked stage which can be described as a short stage due to the sudden failure, The connection between load and slip was straight, but the gradient became less as the load got more. Beyond this point, the gradient flattened down significantly, leading to a growing amount of slip with each successively heavier weight. The test of results obtained for all specimens are listed in Table (4-3) and discussed in the following sections. All of the testing samples behaved elastically to initial, light loads and showed no signs of cracking. Deformation was proportional to the stresses. Eventually, additional fractures appeared as the load increased. In general,

there were two sorts of created cracks, flexural cracks, and shear cracks. At ultimate failure stage the flexural cracks remained fine and failure was characterized by widening of one or more shear cracks. Failure was defined when the load cannot be increased further.

4.4.1 Control specimen (CS)

This specimen was monolithic without any joint, which regarded as reference specimen, see Figure (3-2). Early first flexural crack formed at load about (95 kN) (29 % of the maximum load). After increasing the load level, first shear crack formed at the shear plane (140 kN) (43% of the ultimate load) due to the effect of high shear forces. As the load increased more cracks developed in the shear plane. At load level 320 kN the shear failure, as shown in figure (4-2). Figure (4-3), demonstrates the load-slip curve for this specimen.
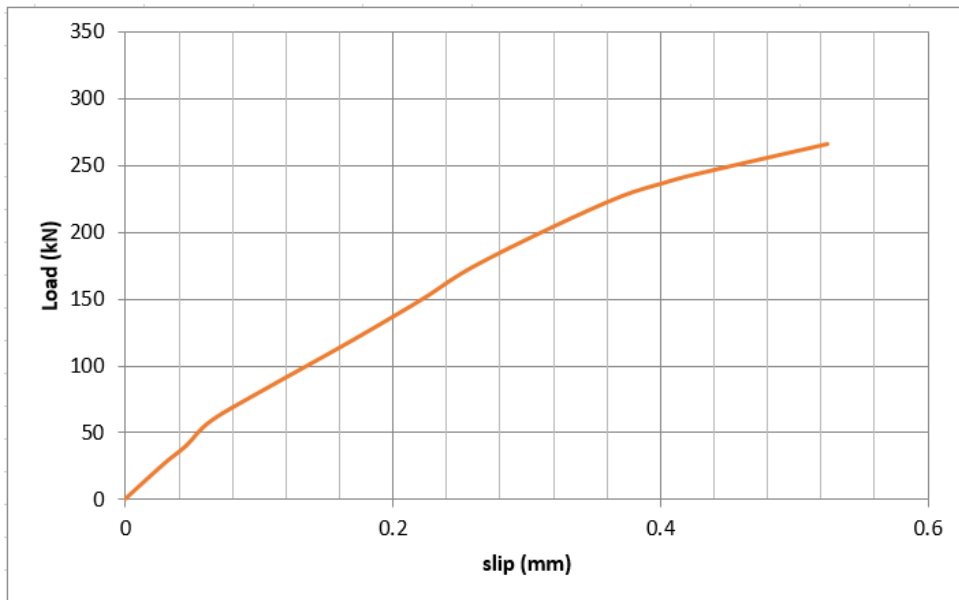
Figure 4- 2. Load-Deflection curve for specimen CS.

Figure 4- 3. Failure mode for CS.

4.4.2 First group grooves specimens

In this group, all the groove specimens (rectangle grooves, circle grooves, and triangle grooves) are discussed. The variable adopted here included type of interface. The influence of interfacing has been studied through cracking load, ultimate strength and failure mode and compared the results with those of reference specimen.

4.4.2.1 RG specimen

The specimen RG (rectangle grooves specimen). The first flexural crack formed at the load about (82 kN) (i.e., 51 % of the ultimate load). After increasing the load level, first shear crack formed from the bottom of the shear plane of the first part at load (100 kN) (62.5% of the ultimate load) due to the effect of high shear forces. As the load increased to (140kN) another crack formed at the top of the second part. At load level

(160 kN), the specimen fails due to fracture of rectangle grooves at the interface shear plane. As shown Figure (4-4) and Figure (4-5).
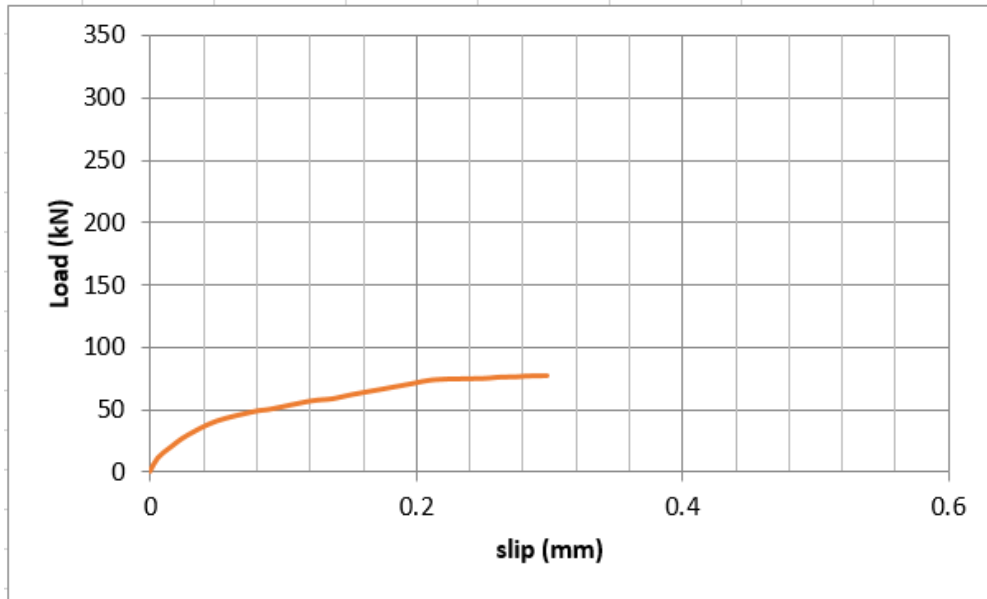
Figure 4- 4.Load-Slip curve for specimen RG.

Figure 4- 5.Failure mode for RG specimen.

4.4.2.2 CG specimen

For this specimen, the first flexural crack formed at the load about (34 kN) (i.e., 44 % of the ultimate load). After increasing the load level, first shear crack formed at the first part of shear plane at load about (50 kN) (65% of the maximum load) due to the effect of high shear forces. As the load increase to (54kN) crack formed in another part. then the shear failure happened at the ultimate load of (77 kN) as shown in Figure (4-7). The circle grooves in the specimen reduces the shear strength when likened with that of the control sample by about (75%) due to reduction in the stiffnes at the shear plane. Figure (4-6) shows the load-slip curve for this specimen.
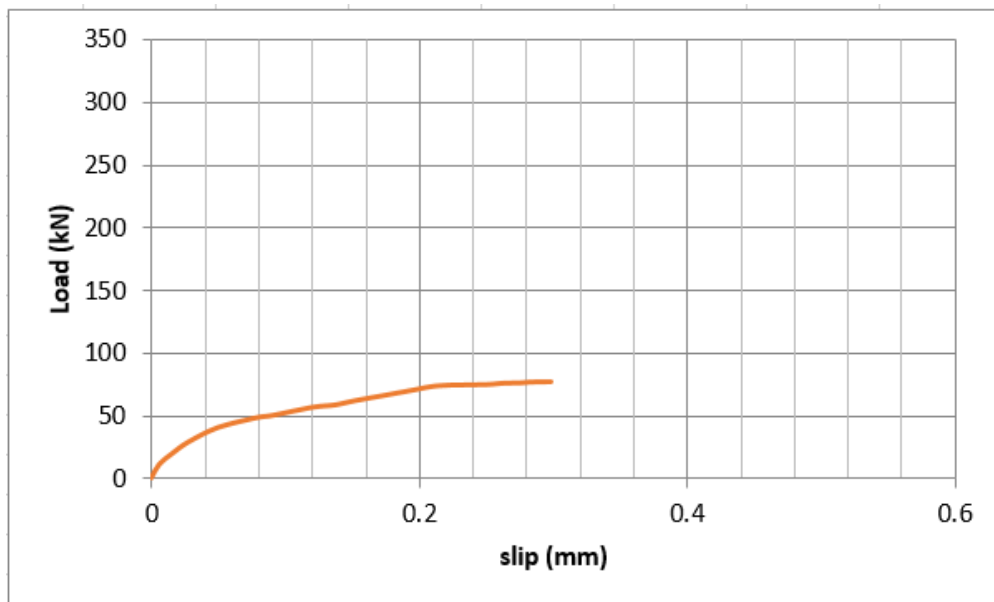
Figure 4- 6.Load- Slip curve for CG specimen.

Figure 4- 7. Failure mode CG specimen.

4.4.2.3 TRG-25 specimen

This specimen TG25 (triangle grooves 25mm) have details as shown in Figure (3-5). Cracks are first observed at the shear plane at about 30 kN, due to stress concentration. No flexural cracks are noted in this specimen. When the load increases, cracks widen rapidly and the two parts start to spread. Then, the specimen failed by the slipping of the two parts, as shown in Figure (4-9). It can be concluded that the triangle interface in the specimen TG25 reduces the shear strength when associated with that of the control case by about (85%), and (71%) less than RG. Figure (4-8) shows the load-slip curve for this sample.
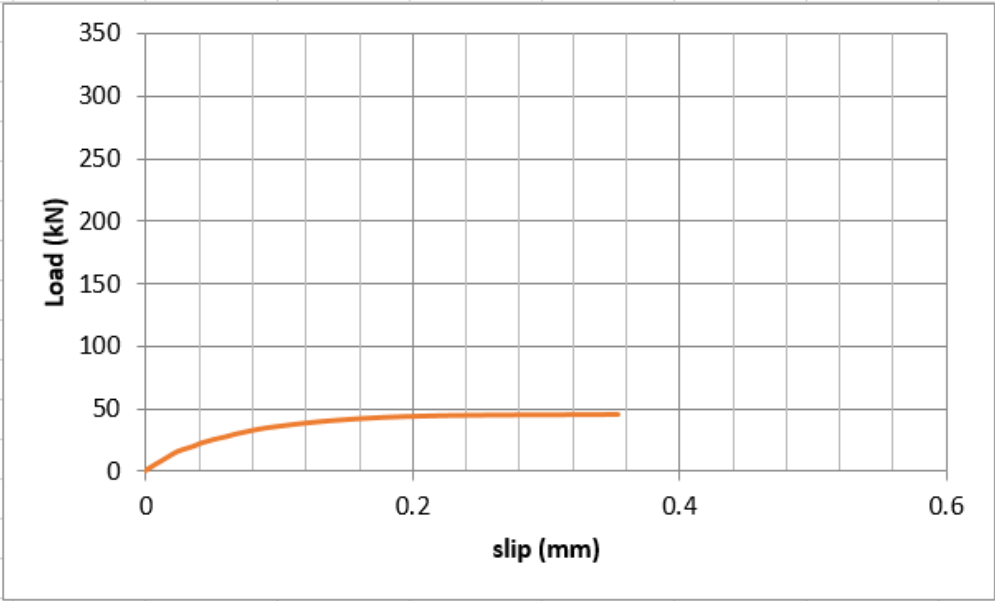
Figure 4- 8.Load- Slip curve for TG25 specimen.

Figure 4- 9.Failure mode TRG 25 specimen.

4.4.2.4 TRG-35 specimen

In this specimen, no flexure cracks are formed. At the load of (30 kN) (44 % of the ultimate load) the shear crack is formed at the shear plane. After increasing the load level. As the load increase the shear cracks become wider. At load level (67 kN), the shear failure occurred by slipping of the two parts as in TGS-25 specimen as shown in Figure (4-11). It can be concluded that the ultimate load which is lower than ultimate load of the control specimen (79%) and lower than RG specimen (58%) increase compared with TG25 specimen. Figure (4-10) shows the load-slip curve for this specimen.
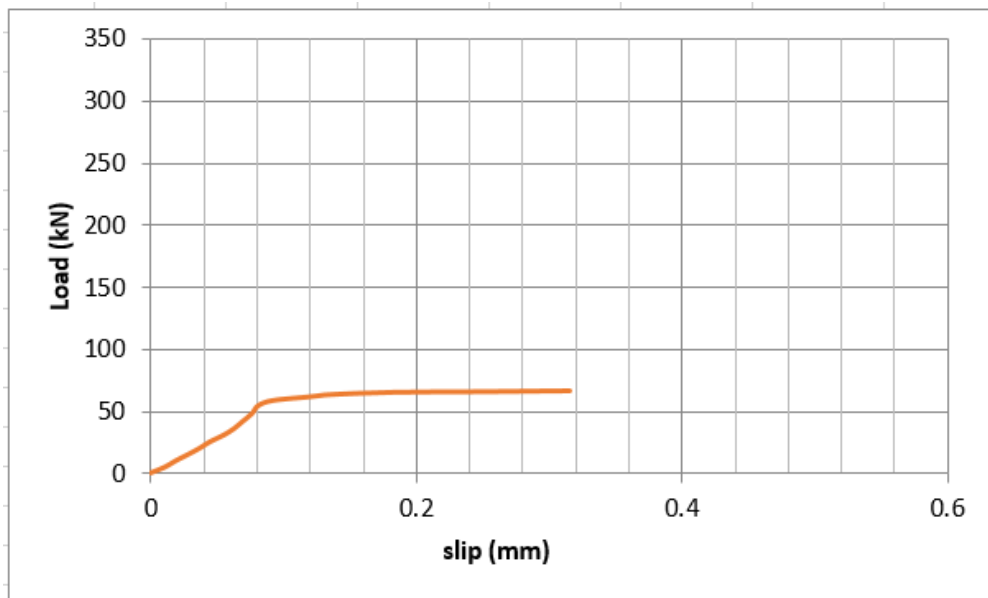
Figure 4- 10.Load- Slip curve for TG35 specimen.

Figure 4- 11.Failure mode TRG 35 specimen.

4.4.3 Second group dowel bars specimens

In this group, two dowel bars specimens (DB1, DB3). The variable adopted here included the type of interface. The influence of interfacing has been studied through cracking load, ultimate strength and failure mode and compared the results with those of control specimen.

4.4.3.1 DB1 specimen

The ultimate load recorded for DB1 specimen (one stirrups with two legs) specimen is 46 kN. Figure (4-12) shows typical load- slip behavior of this specimen. Initial cracks were observed at the shear plane at load 20 kN which is 43% of the ultimate capacity. Maximum capability was almost 85% smaller in the DB1 case compared to the control sample. With the increase in the applied load the cracks become wider and the specimen richs its ultimate capacity and fails due to dowel bars failure. As shown in Figure (4-13).
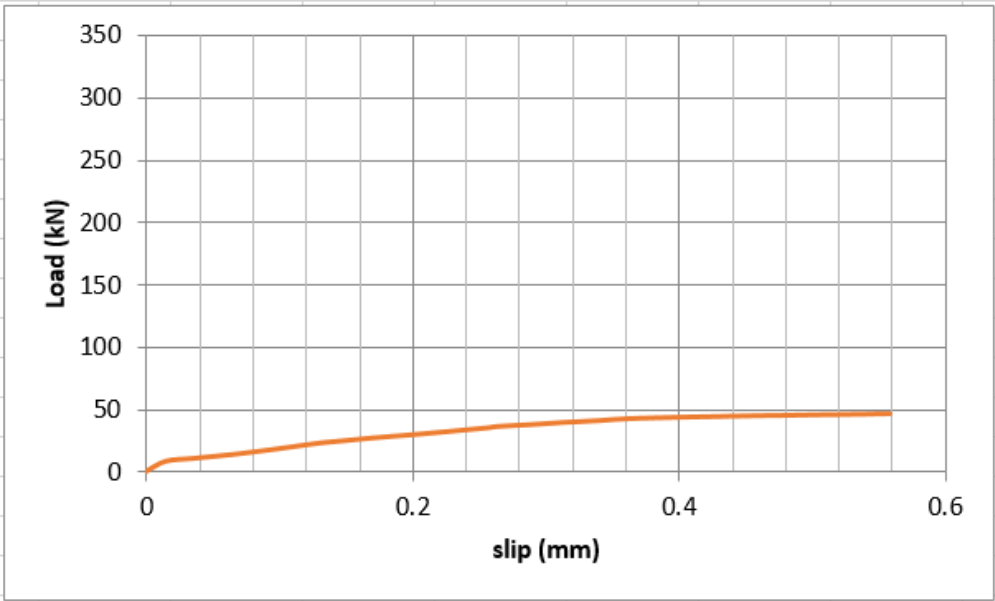
Figure 4- 12.Load- Slip curve for DB1 specimen.
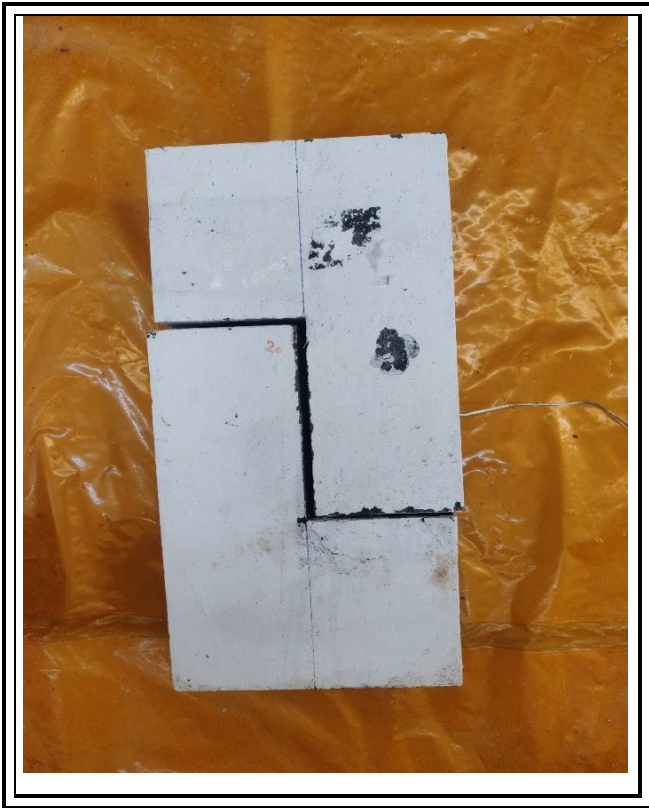
Figure 4- 13.Failure mode DB1 specimen.

61

4.4.3.2 DB3 specimen

DB3 specimen (three stirrups each with two legs) profiles of load versus deformation for such testing are shown in Figure (4-14). When compared to all-UHPC cases, the load-slip curves of the DBS3-reinforced specimens show a trend toward more tiny changes in gradient. This could be due to dowels distribute force more gradually. No flexure cracks occur at the flexure zone. For this specimen the initial crack was observed at load 37 kN which is 57% of the ultimate load. At load of 64 kN the shear failure occurred by failure of the reinforcement, as shown in Figure (4-15). It can be concluded that the ultimate load which is lower than ultimate load of the control specimen (80%) and higher than DB1 specimen about (31%) increased as the dowel bars increased.
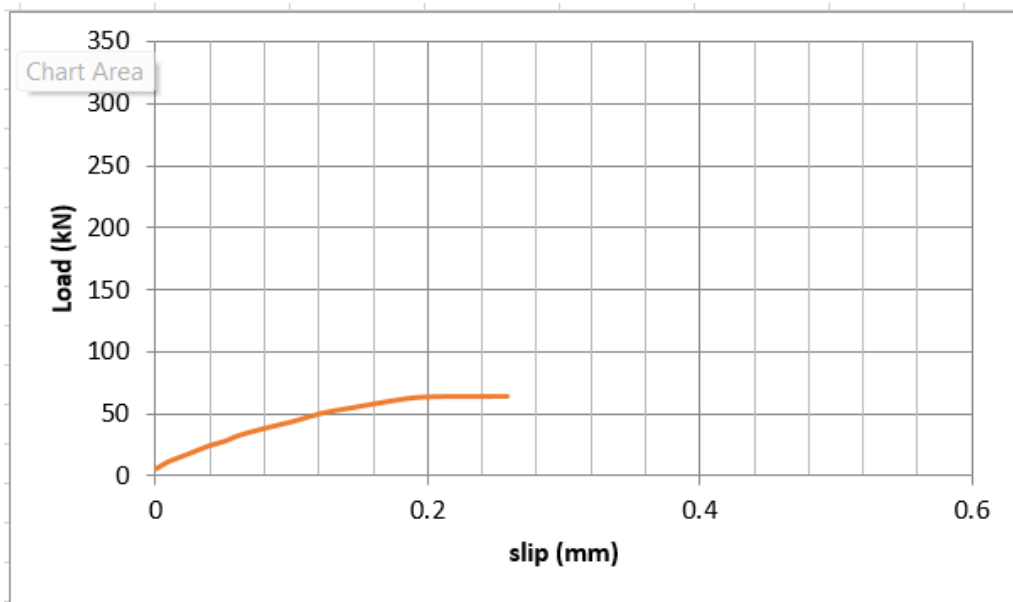
Figure 4- 14.Load- Slip curve for DB3 specimen.

Figure 4- 15.Failure mode for DBS3.

4.4.4 Third group exposed fiber specimens

Two exposed fiber specimens were cast and subjected to granular material at the shear plane in order to investigate the effect of texture on the shear behavior as shown in Figure (4-17). It is important to note that in UHPC-class materials, fibers tend to align with the direction of flow). Specimens were cast by pouring fresh UHPC from one side of the mold and letting it freely flow to the other side of the mold until the mold was full. Thus, fibers likely showed a preferential orientation, which would have been perpendicular to the direction of loading. The shear plane strength may be significantly improved by the addition of steel fibers. The two specimens behave similar in term of ultimate load and load-slip curve. The first crack observed at load 10 kN which is 62% of the ultimate load. Then the specimens fail at about 16 kN. Compared with control specimen the ultimate load of EXF specimens is lower about (95%). Figure (4-16) shows the load-slip curve for this specimen.
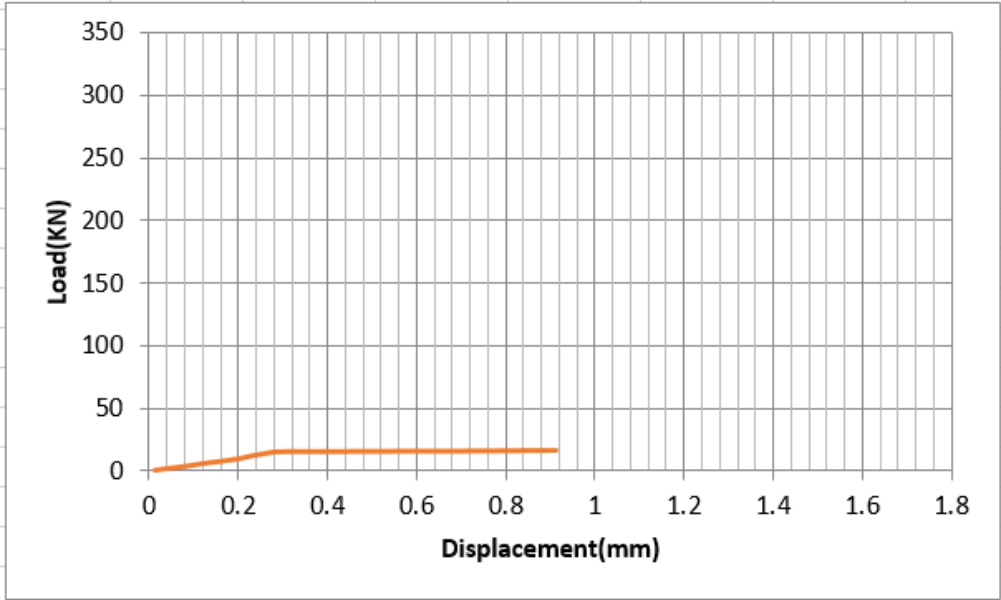
Figure 4- 16.Load- Slip curve for EXF specimen.

Figure 4- 17.Failure mode for EXF specimen.

64

4.5 Effect of interfacing types on structural response

A summary for effect of considered variable (interfacing types) will be discussed and devoted on the main structural response such as the first cracking loads of flexural and shear cracks, ultimate load, slip at service load, failure, as presented in Table (4-4).

4.5.1 Cracking Load

The first crack was a flexural crack formed at the flexural zone except for control specimen (CS) as well as the rectangle groove specimen (RG), and for circle groove specimen (CG). While the first crack at shear plane can be seen for all other specimens (dowel bars group, exposed fiber group and triangle groove specimens). These fissures ranged in length from 25 millimeters to 150 millimeters and were angled at 30 degrees from the vertical and horizontal shear planes. This performance was similar to what was experimental by (Mattock and Hawkins, 1972, Kahn and Mitchell, 2002). In general, it is observed that the first crack at the shear plane formed due to the high-stress concentration. It can also be noticed that specimens reduce the crack load in comparison with control specimens. It can be noted that the rectangle grooves reduce the crack load compared to control specimen by about (13% for flexural crack and 28% for shear crack). On the other hand, the circle grooves specimen exhibited high difference in comparison to control specimen by about (64% for flexural crack and 64% for shear crack). For exsposed fiber interface the shear crack load was less than the shear crack for control specimen by about (92%). It was found that both DB1 and DB3 specimens significantly reduce the first cracking load at the shear plane related to control specimen 85%and73% respectively for shear crack.

4.5.2 Ultimate Strength

For the results of first group the ultimate load capacity for each tested specimen and the comparison with the control specimen are listed in Table (4-3). It is notably that the value of reduction in the ultimate load for RG, CG, TG25, TG35 is 50 %, 75 %, 85

%, and 79 % respectively, while the reduction in the load for second (DB1 and DB3) is 85%, and 80 % respectively. For the water jet group reductions is 95% compared to control specimen. It is clear from the above percentages that the reduction in specimens with groove interface is lower than the corresponding percentages for dowel bars specimens and also the water jet specimens. The reason for this is related to the fact that the grooves interfacing maybe act as a unit.

4.5.3 Cracking pattern and Failure Modes

As previously explained, all push-off specimens were designed to fail by shear. During the tests, this failure mode was clearly obtained. The specimens are breaking into two parts when the cracks increase in the shear plane and the specimens richs its ultimate capacities. For the rectangle and circle grooves specimen (RG and CG specimen), the observed failure mode is due to the fracture in the grooves in the two parts of specimen. Specimens with triangles grooves (TG25 and TG35 specimen) the failure mode was due to slipping of the two parts of the specimen. For the specimens with interface reinforcement the failure was due to the dowel failure.

4.5.4 Ductility index

The capability to endure inelastic deformations before failing under a given load called materials ductility. The present research evaluates ductility factors by dividing the vertical slip at the highest load by the vertical slip at the service load (Russell, 2003).

Table 4-4. Ductility factor (μ) for the tested specimens.

Specimen ID	Service slip (mm)	Ultimate slip (mm)	Ductility index(μ)
CS	0.29	1.40	4.8
RGS	0.075	0.25	3.3
CGS	0.07	0.30	4.3

TGS25	0.085	0.35	4.1
TGS35	0.065	0.31	4.7
DB1	0.18	0.56	3.1
DB3	0.08	0.26	3.25
EXFS1	0.2	0.91	4.55
EXFS2	0.2	0.91	4.55

* Assumed service load = Ultimate load / 1.7 (Mansur, 2006).

From Table (4-4), it can be noticed that the use of rectangle grooves causes a decrease in the ductility by about (31%) when compared to the control specimen. This reduction in the ductility is due to the weakness in interfacing. The decrease in the ductility by 10%,14%,2% for specimens with circle, triangle 25mm, triangle 35mm grooves respectively when compared with the control specimen, this reduction in the ductility is due to increase the slip at the service stage and the reduction in the ultimate load capacity. For the dowel bars specimens (DB1, and DB3 specimens) when compared with the control specimen dowels caused decrease in the ductility by 35%, 32%. And it can be noticed that the dowels number affects very slightly on ductility. While for the expose fiber specimens, the ductility is decreases, decrement in the ductility with related to these specimens can be attributed weak in the bonding of the two parts of the specimen.

4.6 Applicability of ACI 318 (2019) and AASHTO LRFD (2007) code equations for shear friction of UHPC

To measure the amount of shear transfer resulting in a certain plane, the notion of shear friction employs the concept of a coefficient of friction, such as an existing or potential crack, an interface between dissimilar materials, or an interface between two concretes cast at different times. The current ACI shear friction equations is:

$$Vn = \mu Avf fy \qquad\qquad 4\text{-}1$$

not greater than the smaller of:

$$0.2 f_c A_{cv} \qquad\qquad 4\text{-}2$$

$$(480 + 0.08 f_c) A_{cv} \qquad\qquad 4\text{-}3$$

$$or \ 1600 A_{cv} \qquad\qquad 4\text{-}4$$

where

μ = coefficient of friction

A_{vf} = area of rienforcement in mm^2

f_y = yield stress in MPa

f'_c = strength of concrete in MPa

A_c = contact area in mm^2

The AASHTO equation is:

$$V_{ni} = c A_{cv} + \mu(A_{vf} f_y + P_c) \qquad\qquad 4\text{-}5$$

not to exceed the smallest of:

$$K_1 f_c A_{cv} \qquad\qquad 4\text{-}6$$

$$and \ K_2 A_{cv} \qquad\qquad 4\text{-}7$$

where

V_n = nominal shear strength, lb

c = cohesion factor,

For a clean concrete surface, not roughened 75 psi (0.52 MPa).

According to the magnitude of a textured surface 280 psi (1.9 MPa).

For monolithica concrete 400 psi (2.76 MPa).

A_{cv} = zone of concrete thought to be involved in shear transmission at the interaction (b$_v$id$_v$), in^2.

μ = friction factor.

According to the magnitude of a textured surface 1.0.

For a not intentionally roughened surface 0.6.

For concrete cast monolithically 1.4.

Av = area of interface shear reinforcement crossing the shear plane within the area Acv, in2

fy = yield stress of transverse reinforcement, psi

Pc = permanent net compressive force normal to the shear plane, lb

bvi= interface width considered to be engaged in shear transfer, in.

dv= the distance between the centroid of the tension steel and the mid-thickness of the slab to compute a factored interface shear stress.

K1 = concrete cohesion term that is related to strength,

0.3 for cast in place slab cast against roughened girder 0.25 for normal weight concrete placed monolithically, normal weight and lightweight concrete with a roughened surface, 0.2 for normal weight concrete placed against non-roughened surface or cast against studded steel girders

K2 = maximum allowable interface stress

for normal-weight concrete deck cast against roughened girder 1.8 ksi.

for normal-weight concrete cast against roughened concrete or placed monolithically 1.5 ksi.

for lightweight concrete deck cast against roughened girder 1.3 ksi.

for lightweight concrete cast against roughened concrete or placed monolithically 1.0 ksi.

for concrete cast against studded steel girders 0.8 ksi.

4.7   Comparison with Code Equations

Table 4-5.Comparison with Code Equations.

Specimen ID	Test value V*exp* (kN)	ACI Predicted Eq. (kN)	AASHTO predicted Eq. (kN)
CS	**320**	**-**	**50**
RGS	**160**	**-**	**9.3**
CGS	**77**	**-**	**9.3**
TGS-25	**45**	**-**	**14.05**
TGS-35	**67**	**-**	**14.05**
DBS1	**46**	**14.4**	**9.4**
DBS3	**64**	**43.23**	**10**
EXFS1	**15**	**-**	**35**
EXFS2	**14.3**	**-**	**35**

In accordance with the table shear forces are all more than what would be expected from formula 4-1 with a friction factor of 0.6. The findings are conservatively estimated using the AASHTO equations.

**Chapter Five: Finite Element Results And Parametric Study**

5.1 General

Finite element analysis (FEA) is a powerful and inexpensive tool for investigating the non-linear structural behavior of any construction part, including but not limited to RC structures. One of the most widely used commercial finite element analysis packages, ABAQUS is used to analyze structural behavior and conduct parametric investigations. This study used ABAQUS/CAE 2007 (Systèmes, 2007) to do a numerical simulation of the S-shaped shear friction experienced by UHPCs. The most accurate method for investigating the behavior of concrete structures, experimental test has a few disadvantages. The fundamental problem is that there may be variations in experimental outcomes between tests. Furthermore, there are constraints, costs, and delays associated with conducting experiments. Consequently, FE simulation is a crucial method not just for verifying the accuracy of the data, but also for conducting a parametric investigation of numerous factors that were overlooked during the research. This section will compare the numerical findings with the experimental ones for all examined cases to confirm the correctness of the Finite element analysis. The produced FE model and its characteristics would be outlined first. All component's element sorts, nonlinear constitutive model, mesh size, and boundary conditions must be specified. At last, a large-scale parametric investigation will be executed.

5.2 Element type and material properties

It is suggested that concrete be modeled using an eight-nodded linear 3D brick solid element with reduced integration in order to mimic the genuine behavior of an S-shape. This will allow the behavior to be modeled accurately. (C3D8R) (Bahij et al., 2018), as shown in Figure (5-1a). This element type gives a suitable solution for the majority of different applications. Each three-dimensional solid element comprises eight nodes, and each node has three degrees of freedom. It is applicable for linear as well as more complicated nonlinear analyses that take into account contact, plasticity,

and massive deformations. On the other hand, 2-nodded linear truss elements (T3D2) as shown in Figure (5-1b) was used to model steel bars reinforcements. Similar to concrete beam, the three-dimensional solid element (C3D8R) was chosen to model the steel plates in both loading and supporting positions.
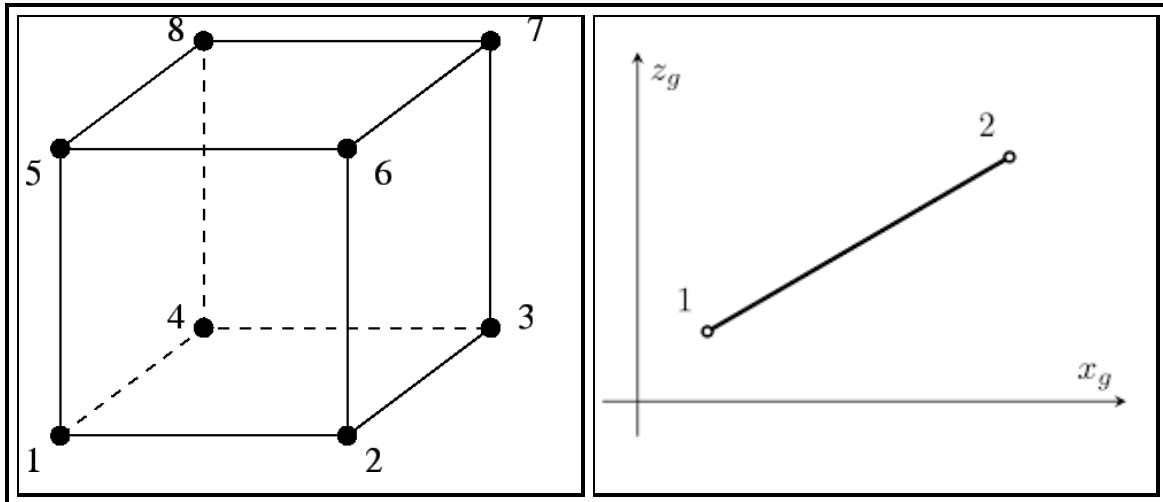
(a) C3D8R element   (b) T3D2 truss element

Figure 5- 1. C3D8R, and T3D2 elements used ABAQUS.

5.3 Materials

Throughout this analysis, concrete damage was modeled using the ABAQUS software and the concrete-damaged plasticity (CDP) model. The tensile cracking failure and compressive crushing failure of concrete, as well as their respective specifications, are provided by this model(Yang et al., 2007). The variables used for the general CDP model are detailed below. For this simulation, the used values of 36 for the dilation angle, 0.1 for the flow potential eccentricity, and 0.001 for the viscosity parameter. The proportion of a material's strength in its uniaxial condition relative to its strength in its biaxial state, fb0⁄fc0, was 1.16. Kc, the second stress invariant along the tensile meridian, with a ratio of 0.6667.

5.4 Model geometry and boundary conditions

For the purpose of obtaining an appropriate estimate of the overall behavior and failure mechanism for UHPC shear friction employing S-shape, three-dimensional simulations were carried out. via taking into account the symmetry of the specimens. Figure(5-2) presents a three-dimensional view of the reference specimen's FE geometric model. To model the connection between the concrete and the reinforcement, the embedding technique was used. In this constraint, concrete was used as the host region while steel reinforcing bars were embedded into the concrete. A perfect connection between concrete and steel can be mimicked by applying this restriction. Steel plates in both loading and supporting positions are connected to the specimen using the ''tie'' option. Since FE commercial software can be high demanding in computational time. The specimens had been analyzed using static analysis in ABAQUS/Standard. In the static analysis, load was applied as a concentrated load on the centerline of the upper plates. The applied load was different for the specimens. Figure (5-3) gives details regarding the typical boundary conditions of the specimens used for the simulations.
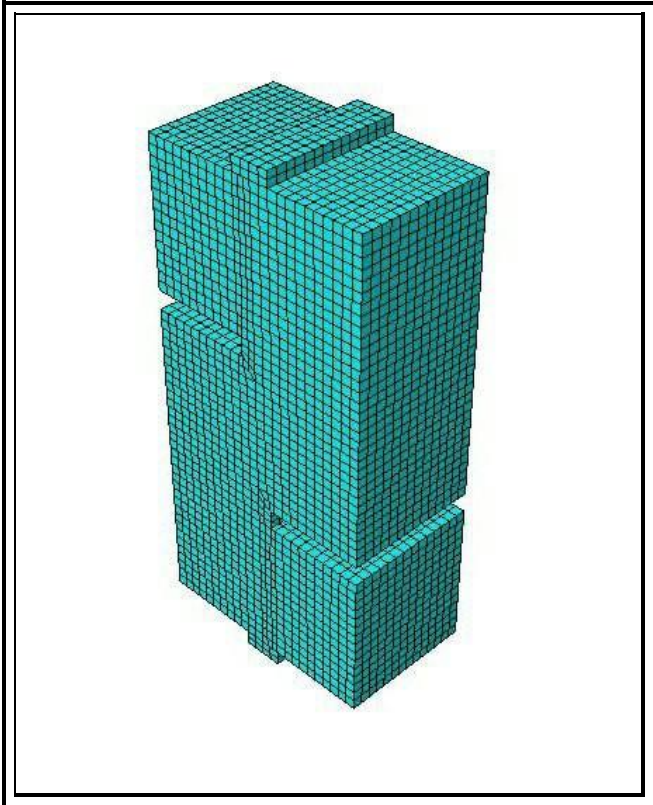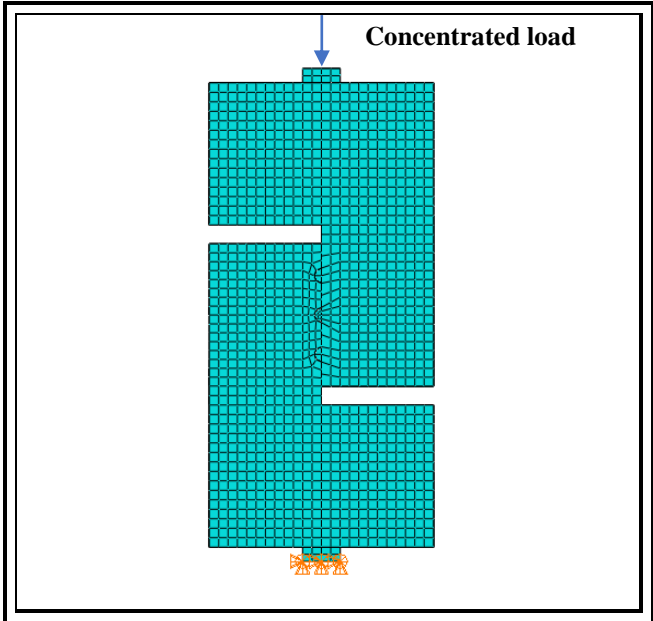
Figure 5- 2. 3D view of the FE model.

Figure 5- 3. Typical applied load and boundary conditions.

75

5.5 Meshing and convergence analysis

Since simulation of cracking is a focus of this study, fine meshing of solid elements would be required to capture directly the progress of concrete cracking. Thus, mesh size in all planes is chosen to be 10 mm. The main aim of the convergence study is to select the proper mesh size of the model with a minimum number of elements and maximum convergence with the results of the experimental test.

5.6 Finite element analysis results and discussion

For each examined specimen, the ABAQUS finite element analysis results are compared with the experimental findings. This comparison establishes the validity of the numerical model in terms of load-slip response, ultimate load-bearing capacity, service slip, cracking pattern, and failure mechanisms, Table (5-1) includes numerical results, of ultimate load and cracking load.

Table 5-1. Numerical results.

Specimen ID	Ultimate load (kN) Pu		Percentage of differences of Pu%	slip at ultimate load (mm)		Percentage of differences of δu%
	EXP	FEM		EXP	FEM	
CS	320	318	0.62	1.4	1.61	-15
RGS	160	172	-7.5	0.25	0.18	28
CGS	77	81	-5.1	0.3	0.2	33
TRGS-25	45	50.5	-12.2	0.35	0.25	28.5

TRGS-35	67	72	-7.4	0.31	0.25	19.35
DBS1	46	51	-10.8	0.55	0.24-	54
DBS3	64	71	-10.9	0.26	0.23	11.5
EXFS	15.77	14.83	5.96	0.91	1.6	-75

5.6.1 Load - slip Response

Figure (5-5) through (5-12) show nine load-slip evaluations, highlighting their key features and the outstanding consistency between experimental data and numerical data for each specimen. The outcomes of the experiments are displayed in orange, while the numerical data from the FE model run in ABAQUS are shown in blue. It seems to be simple to disregard part of the information included in those load–slip statistics as a result of the inconsistent data gathering that occurred throughout the trial experiments. One of them was to identify the differences between each step in the load–slip relation. On the other hand, numerical analysis is a more effective technique for solving problems like this one. In general, each and every one of these quantitative load–slip curves may be broken down into three distinct phases. There was no cracking in the shear plane of the sample throughout Stage One, the linear elastic condition, and relative movement grew proportionally with increasing load. When the connection sample attained Phase 2, the collapse condition, shear fractures developed in the shear plane, the slope of the curve fell to zero, and the load achieved its highest value. Stage one and two roughly followed the same trend in both tests (Rogowsky and MacGregor, 1983) and simulations. Differing from the experimental results, it could be more obvious to distinguish Stage two (the failure state).

Figure 5- 4. Experimental and numerical load-slip curves for CS.

Figure 5- 5. Experimental and numerical load- slip curves for RGS.

Figure 5- 6. Experimental and numerical load- slip curves for CGS.

Figure 5- 7. Experimental and numerical load- slip curves for TRGS-25mm.

Figure 5- 8. Experimental and numerical load- slip curves for TRGS-35mm.

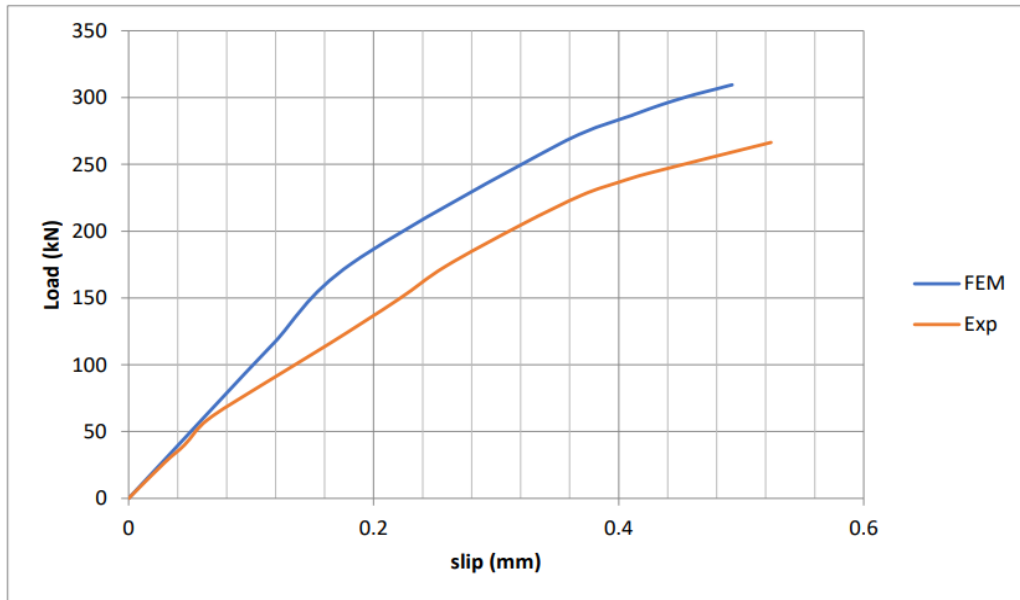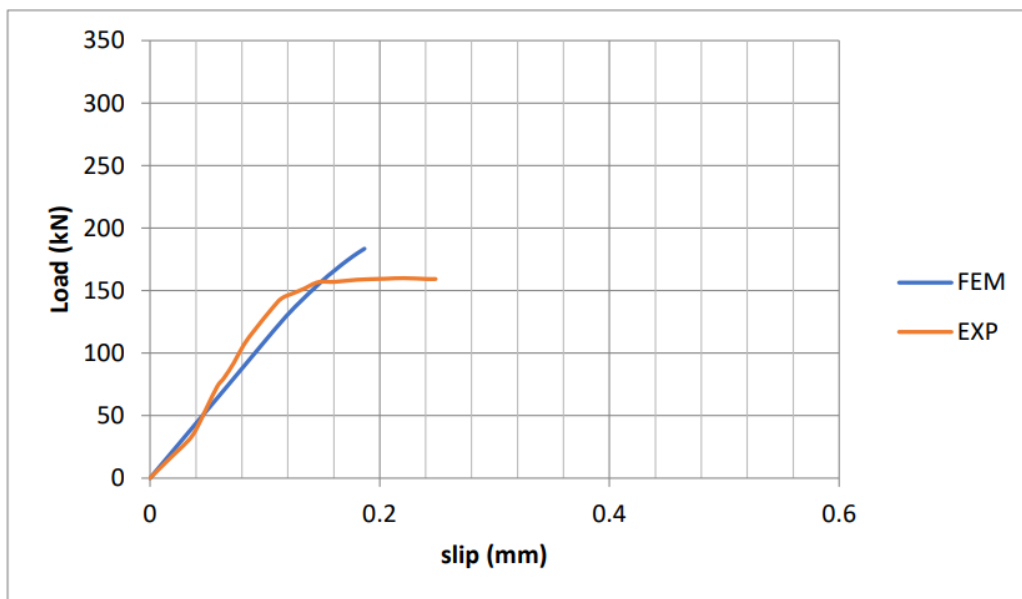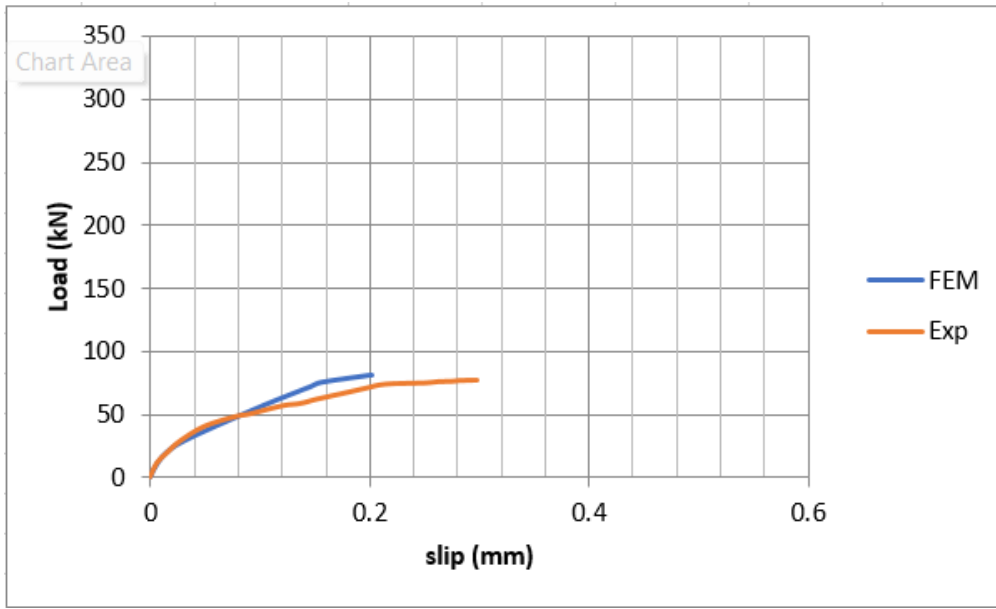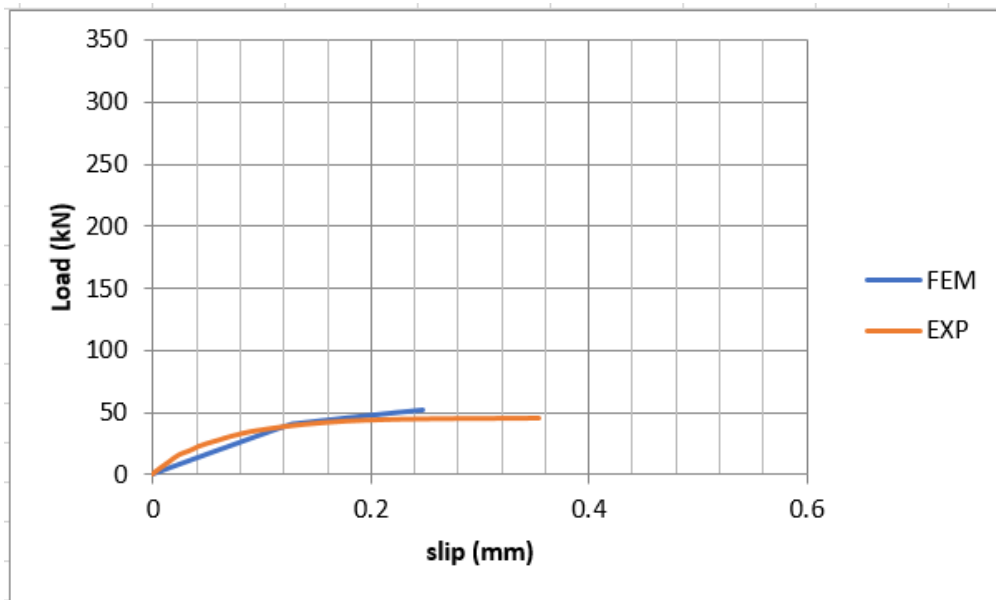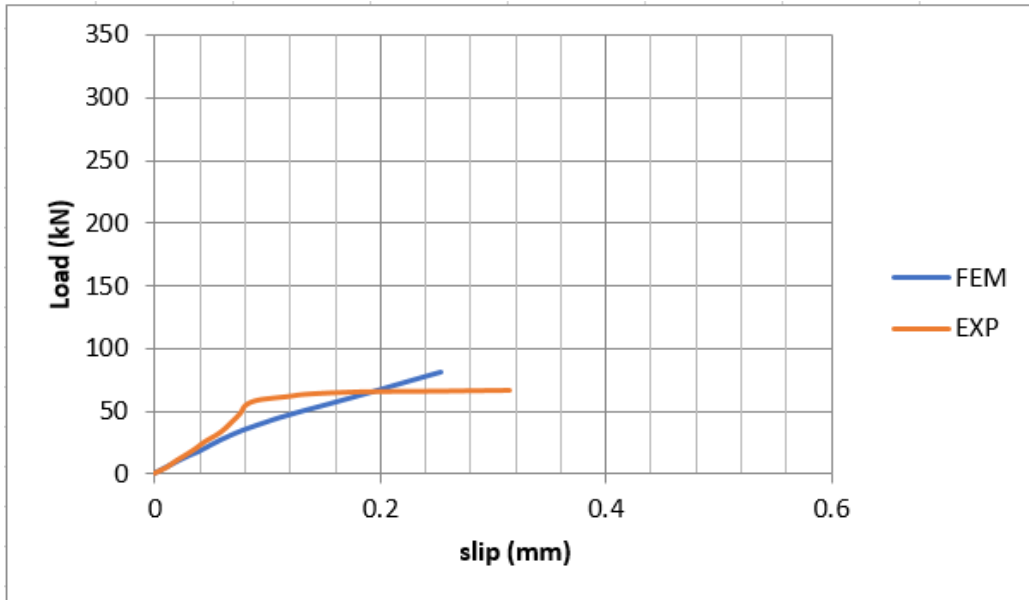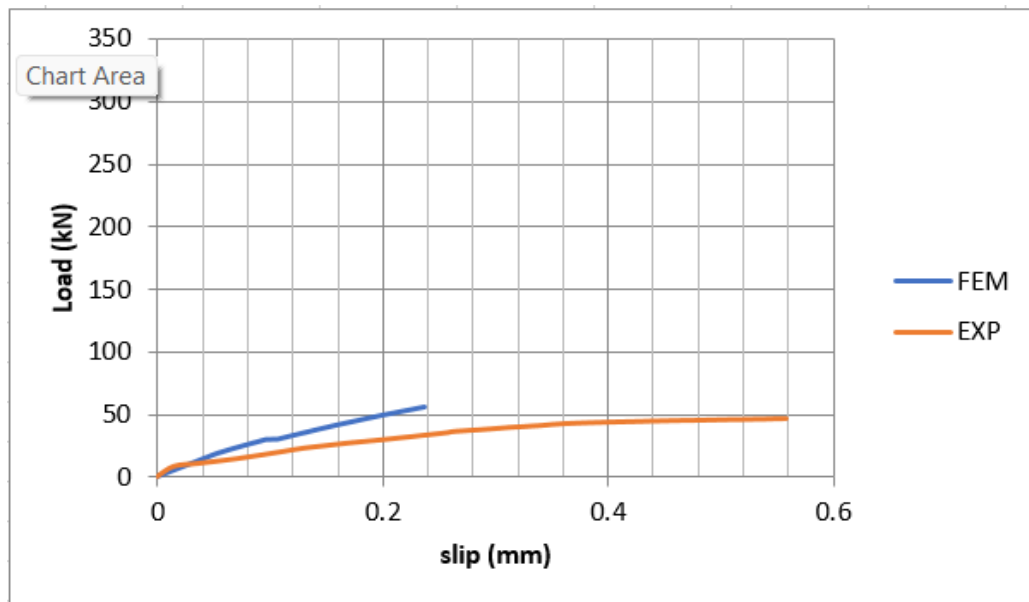*Figure 5- 9. Experimental and numerical load- slip curves for DBS1.*
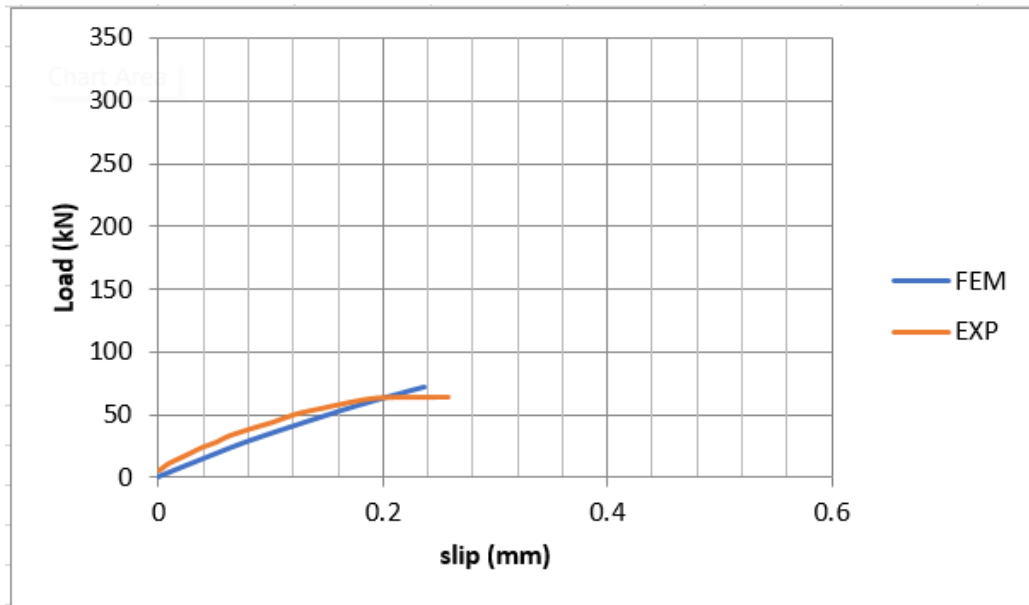
Figure 5-10. Experimental and numerical load- slip curves for DBS3.
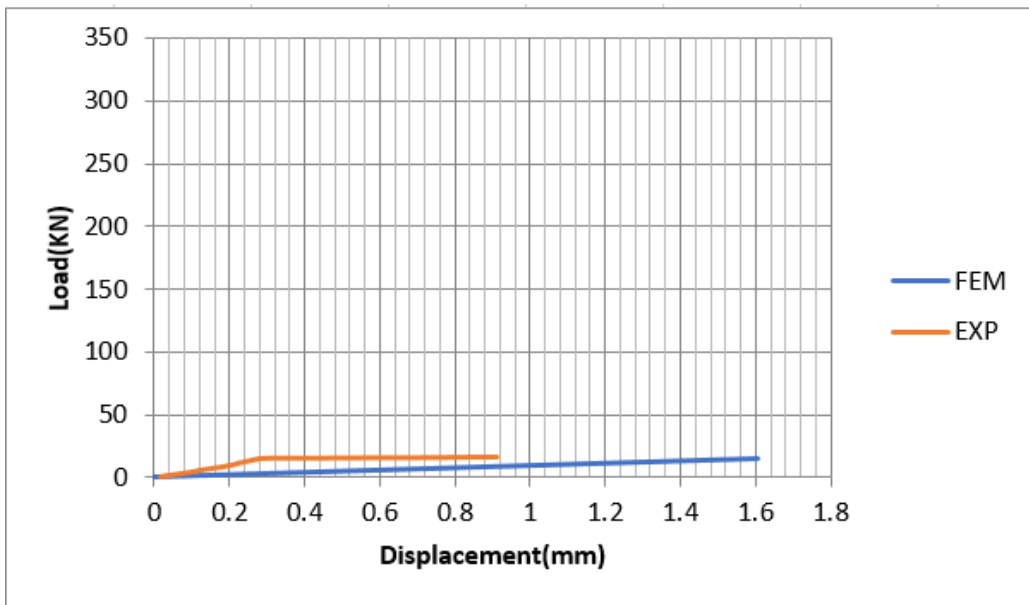
Figure 5-11. Experimental and numerical load- slip curves for EXFS.

5.6.2 Cracking and Ultimate Load

As shown in Table (5-1), FEM and experimental findings are summarized. FEM was capable to capture the minor changes in load–slip response caused by the differences in the interfacing at the shear plane, just as observed in the experimental work. The average difference in results was about 1 % increase in ultimate loads, and a 5% decrease in first cracking loads. However, it can be inferred that the results forecast by FEM were in good agreement with the investigational results.

5.6.3 Slip

As shown in Table (5-1), a comparison between the numerical and experimental slip at the ultimate load for all push-off specimens. The ultimate slip values resulting from the FE analysis gave a reasonable agreement with the experimental values. The average difference in results was about a 9% decrease in the maximum slip at ultimate loads. Figure (5-18) shows profile of the deflected shape for the tested specimens.
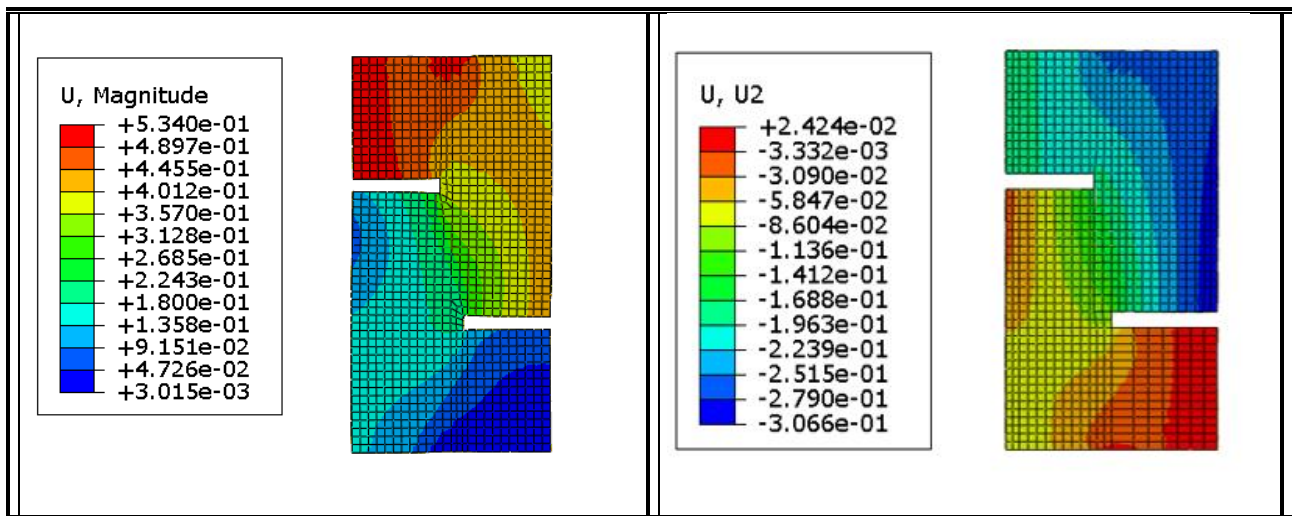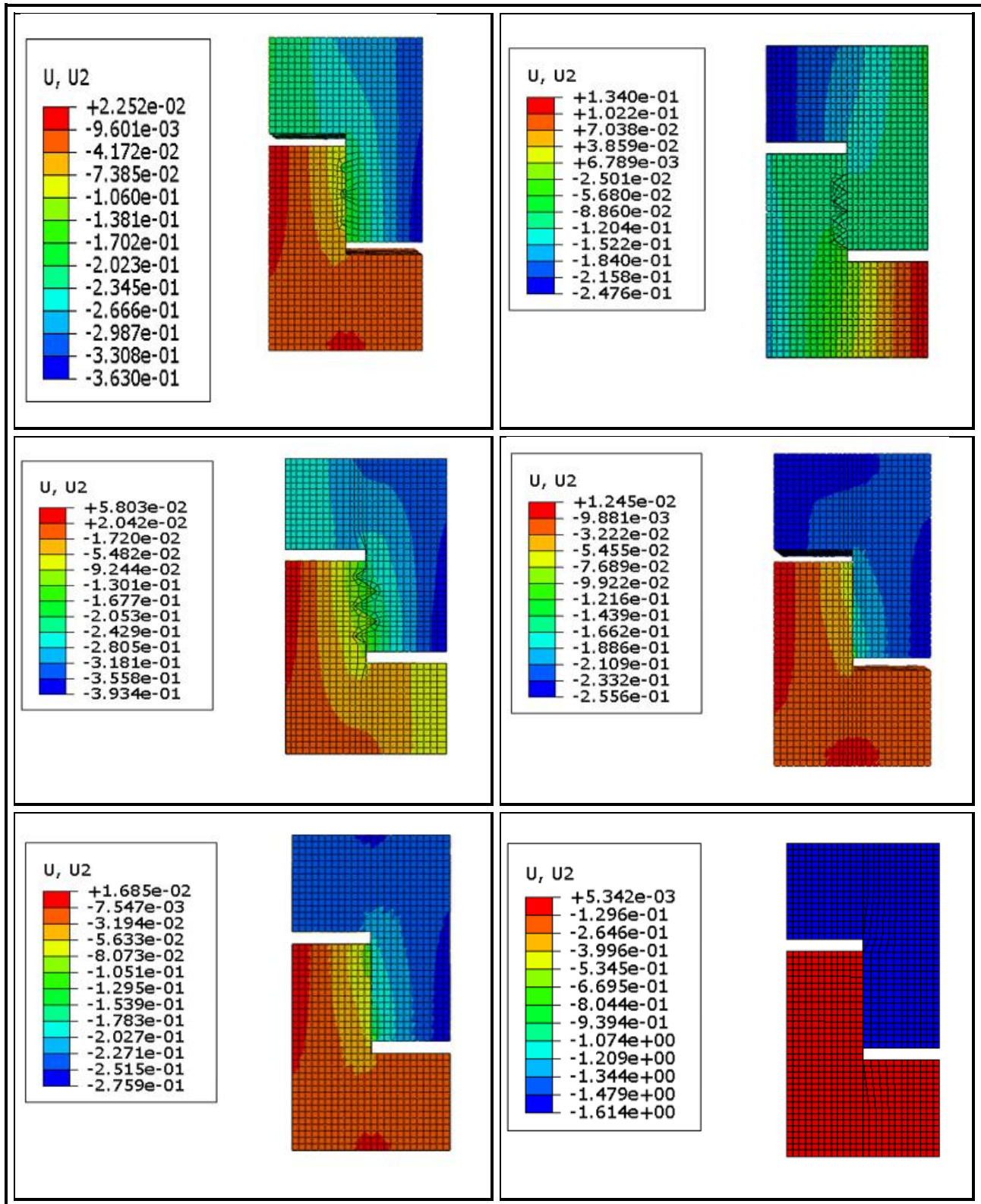
Figure 5- 12. Profile of deflected shape from ABAQUS program for specimens.

5.6.4 Stress Behavior

In this study shear resistance was evaluated using both experimental testing and numerical analysis, two experimental specimens and one numerical specimen are shown for comparison. Since the average and standard deviation are around 98.0% and 7.8%, respectively, the numerical statistics corresponded well with the relevant research observations. The ultimate shear strength could be reliably predicted using the FE model suggested in this investigation.
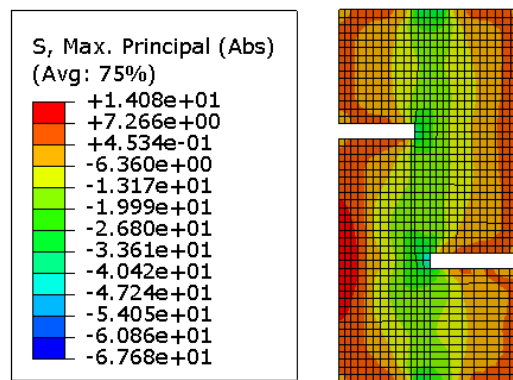
Figure 5- 13. Stresses (σ max principal) distribution of FEM at ultimate load for RGS.
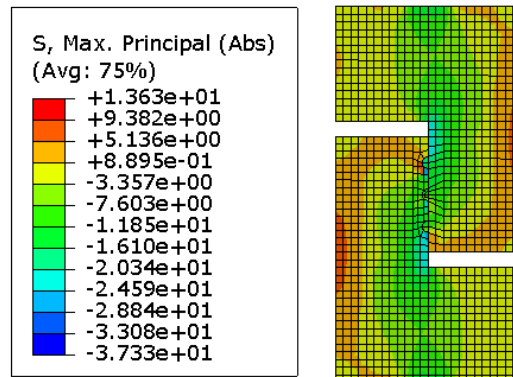
Figure 5- 8. Stresses (σ max principal) distribution of FEM at ultimate load for CGS.
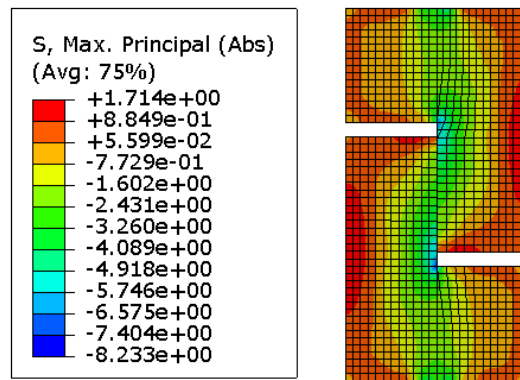
Figure 5- 9. Stresses (σ max principal) distribution of FEM at ultimate load for WJS.
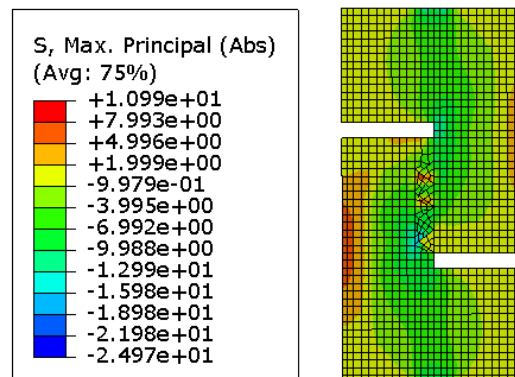
Figure 5- 10. Stresses (σ max principal) distribution of FEM at ultimate load for TGS25.
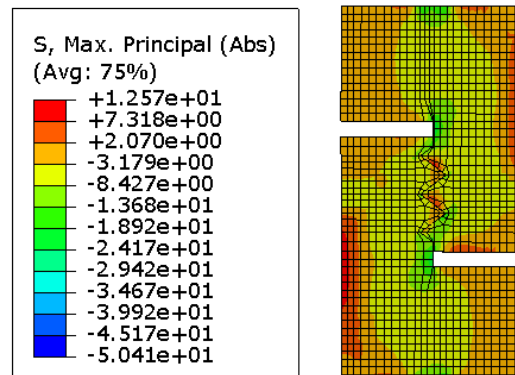
Figure 5- 11. Stresses (σ max principal) distribution of FEM at ultimate load for TGS35.
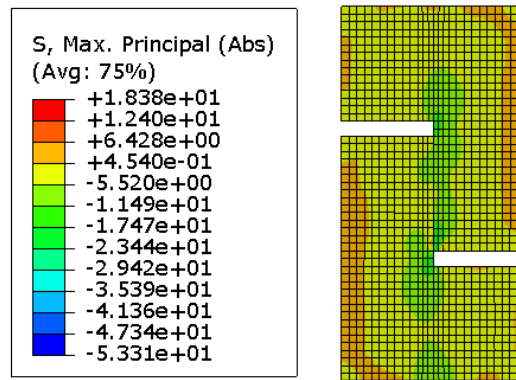
Figure 5- 12. Stresses (σ max principal) distribution of FEM at ultimate load for DBS1.
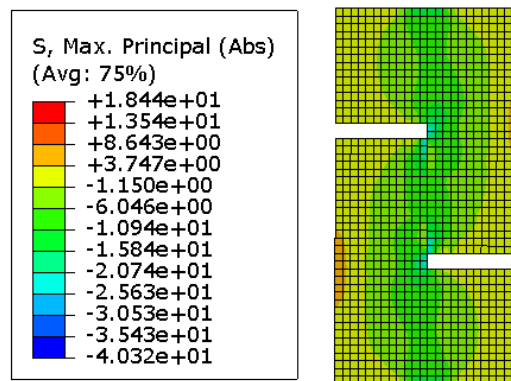
Figure 5- 13. Stresses (σ max principal) distribution of FEM at ultimate load for DBS3

5.7 Parametric study

The parameters investigated in the study include Compressive Strength, Dowel bar effect. Utilizing the FE model developed in this study, which has been shown to be reasonable agreement in predicting cracking load, ultimate load, ultimate slip and damage states. So, a parametric study was performed in order to generate a more detailed and precise understanding of the shear behavior of UHPC.

5.7.1 Compressive Strength of UHPC

Specimens RGS and CGS were investigated with a compressive strength of 200 MPa for UHPC to provide information on the effect of

compressive strength for UHPC. Figure (5-20) and Table (5-2) indicate that the compressive strength of UHPC had a significant impact on the behavior of the two

grooved specimens. An increase in UHPC strength from 120 to 200 MPa resulted in a significant rise in shear capacity (about 37%), as well as an increase in first cracking load and an enhancement in specimen stiffness.

5.7.1.1 Concrete Strength Influence on Shear Capacity and the Load-Slip Relationship

When concrete's strength was increased, both its critical shear strength and preliminary stiffness rose. According to Table (5-2), which compares the impact of increasing concrete strength on ultimate shear strength, the shear capacity of those specimens significantly increased when concrete strength was 200MPa.
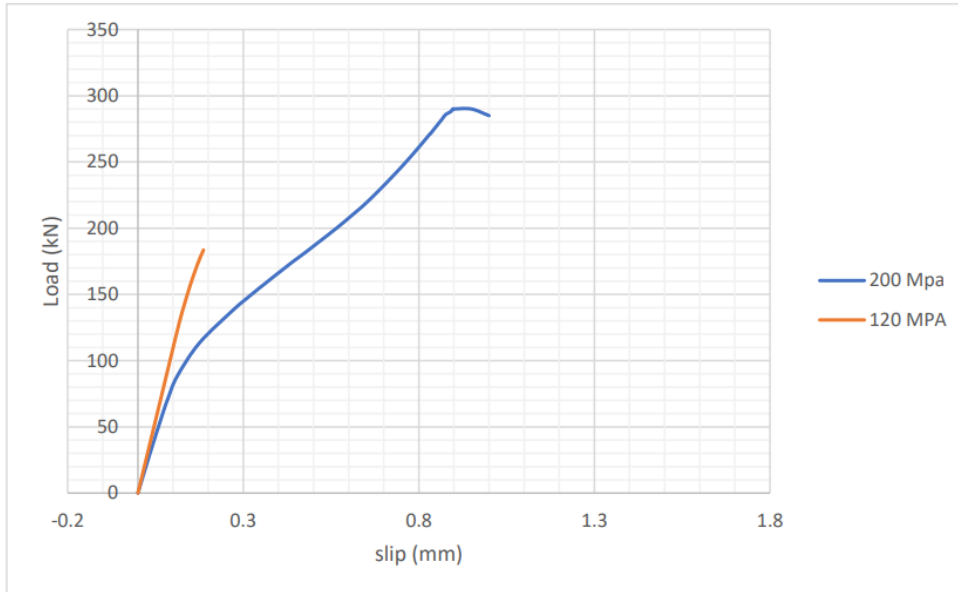
Figure 5- 20. Load–slip curve for 200 MPA RGS
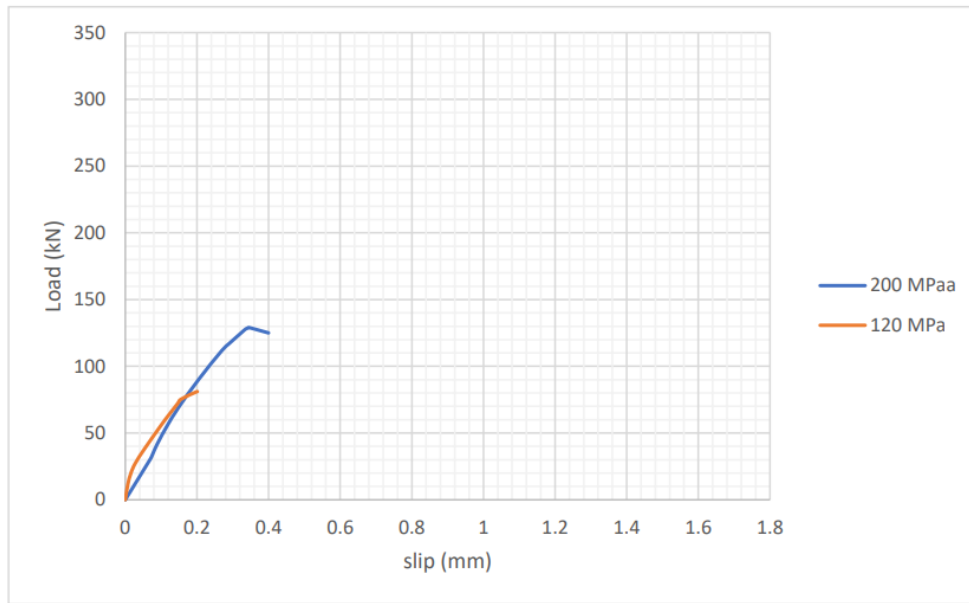
Figure 5- 21. Load–slip curve for 200 MPA CGS

Table 5-2.Effect of Compressive Strength on ultimate load.

Specimen ID	Compressive strength (MPa)	Ultimate load (KN)	COV
RGS	120	183	
	200	292	
CGS	120	81	0.32
	200	130	

5.7.2 Dowel bar effect

A new specimen with two and four dowel bars was investigated in order to provide the required information for the cases that are not investigated in the experimental program. As shown in Figure 5-22 and Table 5-3. It can be seen that using two dowel bars increased the shear capacity of UHPC compared to the DB1 specimen, while using four dowel bars resulted in a significant rise in shear capacity.

5.7.2.1 Effects of dowel bars on Shear Capacity and Load–Slip Relationship

The number of dowel bars increased along with both ultimate shear strength and initial stiffness. According to Table 5-3, which compares the impact of increasing the number of dowel bars on ultimate shear strength, the shear capacity of those specimens increased as the number of bars increased.
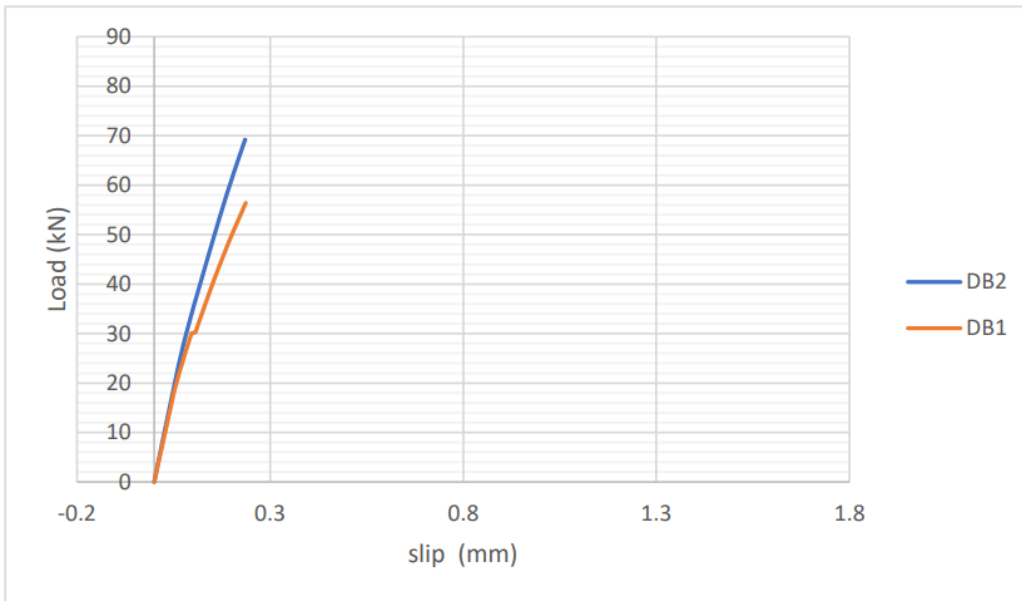
Figure 5- 22. Load–slip curve for DBS2.
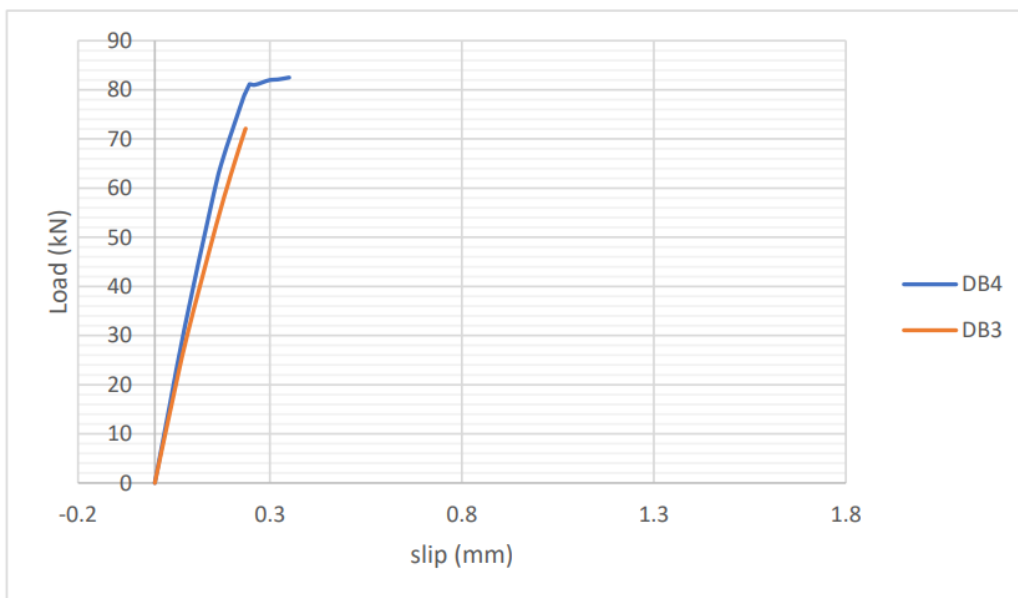
Figure 5- 23. Load–slip curve for DBS4.

Table 5-3.Effect of dowel bars on the ultimate load.

Specimen ID	Ultimate load (KN)	COV
DBS1	51	-
DBS2	69	0.14
DBS3	71	0.03
DBS4	82	0.08

Chapter Six: Conclusions and recommendation for future works

6.1 **General**

In the previous chapters, an experimental work together with a finite element analysis and parametric study were considered for UHPC using push off specimens with different types of interface. Both experimental and numerical results using ABAQUS software showed that providing UHPC have varying effect on the overall behavior and ultimate strength depends on many parameters such as type of interfacing, strength of materials and the shape of the reinforcement. From the experimental and numerical results, conclusions can be drawn in this field as well as some suggestions for future works are presented.

6.2 Conclusions from experimental work

The following was drawn from the findings of the present study of shear fraction in monolithic and cold-joint push-off samples:

1- Shear transmission through extant fractures in monolithic UHPC is significantly enhanced by steel fibers even in the absence of additional shear reinforcement.

2- The contact shear behavior of UHPC was described to be under-estimated using the formulae suggested in the AASHTO and ACI equations.

3- In general, using of grooves leads to a decrease in both first cracking loads and ultimate loads as average about 62% and 72%.

4- Using grooves interface produces discontinuities or disturbances in the normal flow of stresses, thus lead to stress concentration in the shear plane and early cracking at the top and bottom of the grooves.

5- The load-slip line was practically linear up till the peak load is placed; when the maximum load was applied, the relationship decreased, which indicated that the bond strength had been obtained.

6- Increasing the shear reinforcement across the shear plane improves the shear resistance.

7- Increasing the depth of interface may be necessary if exposed fiber is to be used to boost shear strength.

6.3 Conclusions from numerical study

The following conclusions are derived from the 3D Finite Element Analysis based on the CDP model of ABAQUS package as follows:

1- The nonlinear finite element analysis, adopted in this work is validated for the analysis of UHPC push-off specimens. The overall response of load slip curves, the ultimate load, and the slip of the specimens that were analyzed and estimated using FEM were all in fair agreement with the findings of the experiments.

2- The comparison between the experimental and numerical results confirms the validity of the numerical analysis and the methodology developed, where the difference ratio in the ultimate load was between (0.62-12.2) %.

3- Increasing the number of dowel bars greatly affects the load-slip response as well as the ultimate load.

4- Increasing the concrete compressive strength from 120 to 200 MPa improves the load-slip behavior and the ultimate load response.

6.4 RECOMMENDATIONS FOR FUTURE WORKS

The following suggestions for further study are based on the existing literature:

1- The influence of fibre orientation on the compressive and tensile characteristics of UHPC has to be further investigated in a parametric research.

2- It is necessary to link the outcomes of small-scale testing to full-scale constructions.

3- More research is needed to determine the effect of high strength or/and lightweight concrete on the strength and behavior of shear transfer.

4- Usning bonding agency at the interface

References

Akhnoukh, A. K. & Buckhalter, C. 2021. Ultra-high-performance concrete: Constituents, mechanical properties, applications and current challenges. Case Studies in Construction Materials, 15, e00559.

Al-Azzawi, A. A., Ali, A. S. & Risan, H. K. 2011. Behavior of ultra high performance concrete structures. ARPN Journal of Engineering and Applied Sciences, 6, 95-109.

Al-Hassani, H., Al-Shaarbaf, I. & Hannawayya, S. Behavior of Reactive Powder Concrete Beams in Bending. ENGINEERING and DEVELOPMENT, 167.

Anderson, A. R. 1960. Composite designs in precast and cast-in-place concrete. Progressive Architecture, 41, 172-179.

ASTM, C1240. 2020. Standard Specification for Silica Fume Used in Cementitious Mixtures.

ASTM, C39. 2012. Standard test method for compressive strength of cylindrical Concrete specimens.

ASTM, C494. 2013. Standard Specification for Chemical Admixtures for Concrete.

ASTM, C496. 2011. Standard Test Method for Splitting Tensile Strength of Cylindrical Concrete Specimens.

Bahij, s., adekunle, s. K., al-osta, m., ahmad, s., al-dulaijan, s. U. & rahman, m. K. 2018. Numerical investigation of the shear behavior of reinforced ultra-high-performance concrete beams. Structural Concrete, 19, 305-317.

Birkeland, P. W. & Birkeland, H. W. Connections in precast concrete construction. Journal Proceedings, 1966. 345-368.

C1856/C1856M-17, A. 2017. Standard Practice for Fabricating and Testing Specimens of Ultra-High Performance Concrete. ASTM International, West Conshohocken, PA.

REFERENCES

Crane, C. K. 2010. Shear and shear friction of ultra-high performance concrete bridge girders, Georgia Institute of Technology.

Farouk, A. I. B., Zhu, J. & Yuhui, G. 2022. Finite element analysis of the shear performance of box-groove interface of ultra-high-performance concrete (UHPC)-normal strength concrete (NSC) composite girder. Innovative Infrastructure Solutions, 7, 1-18.

Feng, Z., Li, C., Pan, R., Yoo, D.-Y., He, J. & Ke, L. 2022. Shear Capacity of Ultrahigh-Performance Concrete with Monolithic Interface and Wet-Joint Interface. Journal of Materials in Civil Engineering, 34, 04022153.

Fujikake, K., Senga, T., Ueda, N., Ohno, T. & Katagiri, M. 2006. Effects of strain rate on tensile behavior of reactive powder concrete. Journal of Advanced Concrete Technology, 4, 79-84.

Gopal, B. A., Hejazi, F., Hafezolghorani, M. & Voo, Y. L. 2020. Shear Strength of Dry and Epoxy Joints for Ultra-High-Performance Fiber-Reinforced Concrete. ACI Structural Journal, 117.

Haber, Z. B., De La Varga, I., Graybeal, B. A., Nakashoji, B. & El-Helou, R. 2018. Properties and behavior of UHPC-class materials. United States. Federal Highway Administration. Office of Infrastructure ….

Hanson, N. W. 1960. Precast-prestressed concrete bridges: 2. Horizontal shear connections, Portland Cement Association, Research and Development Laboratories Skokie ….

Harries, K. A., Zeno, G. & Shahrooz, B. 2012. Toward an improved understanding of shear-friction behavior. ACI Structural Journal, 109, 835.

Hofbeck, J., Ibrahim, I. & Mattock, A. H. Shear transfer in reinforced concrete. Journal Proceedings, 1969. 119-128.

Iraqi Specification, No. 45/1984, "Aggregate from Natural Sources for Concrete and Construction.,".

REFERENCES

Iraqi Standard Specification, No.5 of 1984 "Portland Cement", The central organization for standardization and quality control.

Jang, H.-O., Lee, H.-S., Cho, K. & Kim, J. 2017. Experimental study on shear performance of plain construction joints integrated with ultra-high performance concrete (UHPC). Construction and Building Materials, 152, 16-23.

Jang, H.-O., Lee, H.-S., Cho, K. & Kim, J. 2018. Numerical and experimental analysis of the shear behavior of ultrahigh-performance concrete construction joints. Advances in Materials Science and Engineering, 2018.

Jiang, H., Chen, M., Sha, Z., Xiao, J. & Feng, J. 2020. Numeric analysis on shear behavior of high-strength concrete single-keyed dry joints with fixing imperfections in precast concrete segmental bridges. Materials, 13, 2914.

Jiang, H., Shao, T., Fang, Z., Xiao, J. & Hu, Z. 2021. Shear-friction behavior of grooved construction joints between a precast UHPC girder and a cast-in-place concrete slab. Engineering Structures, 228, 111610.

Kahn, L. F. & Mitchell, A. D. 2002. Shear friction tests with high-strength concrete. Structural Journal, 99, 98-103.

Kmiecik, P. & Kamiński, M. 2011. Modelling of reinforced concrete structures and composite structures with concrete strength degradation taken into consideration. Archives of civil and mechanical engineering, 11, 623-636.

Li, C., Feng, Z., Ke, L., Pan, R. & Nie, J. 2019. Experimental study on shear performance of cast-in-place ultra-high performance concrete structures. Materials, 12, 3254.

Liu, J., Chen, Z., Guan, D., Lin, Z. & Guo, Z. 2020. Experimental study on interfacial shear behaviour between ultra-high performance concrete and normal strength concrete in precast composite members. Construction and Building Materials, 261, 120008.

REFERENCES

Liu, T., Wang, Z., Guo, J. & Wang, J. 2019. Shear strength of dry joints in precast UHPC segmental bridges: Experimental and theoretical research. Journal of Bridge Engineering, 24, 04018100.

Lubliner, J., Oliver, J., Oller, S. & Oñate, E. 1989. A plastic-damage model for concrete. International Journal of solids and structures, 25, 299-326.

Malm, R. 2006. Shear cracks in concrete structures subjected to in-plane stresses. KTH.

Mansur, M. Design of reinforced concrete beams with web openings. Proceedings of the 6th Asia-Pacific structural engineering and construction conference (ASPEC 2006), 2006. Kuala Lumpur Malaysia, 5-6.

Mast, R. F. 1968. Auxiliary reinforcement in concrete connections. Journal of the Structural Division, 94, 1485-1504.

Mattock, A. H. & Hawkins, N. M. 1972. Shear transfer in reinforced concrete—Recent research. Pci Journal, 17, 55-75.

Mccormac, J. C. & Brown, R. H. 2015. Design of reinforced concrete, John Wiley & Sons.

Muzenski, S., Haber, Z. B. & Graybeal, B. 2022. Interface Shear of Ultra-High-Performance Concrete. ACI Structural Journal, 119, 267-280.
Popovics, S. 1973. A numerical approach to the complete stress-strain curve of concrete. Cement and concrete research, 3, 583-599.

Rahman, A. & Hoque, M. M. 2019. Parameters affecting the interfacial bond between concrete of different ages: a review of literature. Journal of Civil Engineering (IEB), 47, 79-95.

Randl, N. 2013. Design recommendations for interface shear transfer in fib Model Code 2010. Structural Concrete, 14, 230-241.

Rogowsky, D. M. & Macgregor, J. G. 1983. Shear strength of deep reinforced concrete continuous beams.

REFERENCES

Russell, J. S. 2003. Perspectives in Civil Engineering: Commemorating the 150th Anniversary of the American Society of Civil Engineers, ASCE Publications.

Semendary, A. A., Hamid, W. K., Steinberg, E. P. & Khoury, I. 2020. Shear friction performance between high strength concrete (HSC) and ultra high performance concrete (UHPC) for bridge connection applications. Engineering Structures, 205, 110122.

Abaqus analysis user's manual. 2007. Simulia Corp. Providence, RI, USA, 40.

Yang, K.-H., Chung, H.-S. & Ashour, A. F. 2007. Influence of inclined web reinforcement on reinforced concrete deep beams with web openings.

Zheng, W., Li, H. & Wang, Y. 2012. Compressive stress–strain relationship of steel fiber-reinforced reactive powder concrete after exposure to elevated temperatures. Construction and Building Materials, 35, 931-940.

Zhou, X., Mickleborough, N. & Li, Z. 2005. Shear strength of joints in precast concrete segmental bridges. ACI Structural Journal, 102, 3.

Zilch, K. & Reinecke, R. Capacity of shear joints between high-strength precast elements and normal-strength cast-in-place decks. PCI/FHWA/FIB International Symposium on High Performance ConcretePrecast/Prestressed Concrete InstituteFederal Highway AdministrationFederation Internationale du Beton, 2000.

Appendices A

Modeling Of Material Properties In Finite Element Analysis

A.1 Introduction

There are three material models for analyzing concrete in ABAQUS: (1) Smeared crack concrete model, (2) Brittle crack concrete model, and (3) Concrete damaged plasticity (CDP) model. Out of the three concrete models, the concrete damaged plasticity model is selected in the present study. Details of the CDP model used in ABAQUS, in addition to the behavior and properties of the concrete and the other material used in this study are described below.

A.2 Concrete damaged plasticity in abaqus

Concrete damaged plasticity is capable of modelling all structural types of reinforced or unreinforced concrete or other quasi-brittle materials subjected to monotonic, cyclic, or dynamic loads, this model is based on a coupled damage plasticity theory and the multi-axial behavior of concrete in damaged plasticity model governs by a yield surface, which proposed by (Lubliner et al.) (Lubliner et al., 1989). Tensile cracking and compressive crushing of concrete are two assumed main failure mechanisms in this model. Furthermore, the degradation of material for both tension and compression behavior have been considered in this model. Degradation of concrete in cyclic and dynamic loadings is taken into account by defining two scalar parameters; tensile damage parameter (dt) and compressive damage parameter (dc).

A.2.1 Concrete Damaged Plasticity Parameters in Triaxial Loading State

In order to describe strength with the equation for triaxial stress as input to the finite element program ABAQUS, a set of five parameters are required to completely describe the plastic behavior of concrete;

Ψ, Dilation angle: The angle of inclination of the failure surface toward the hydrostatic axis, measured in the meridional plane. Physically, dilation angle Ψ is interpreted as a concrete internal friction angle. Maximum value of it equal (56.3o) and minimum value is close to (zero) (Kmiecik and Kamiński, 2011).Through many trials of geometry with the aim of achieving proper failure to be compatible with the observed experimental failure mechanism, the value of dilation angle was taken as (45°)for NSC and (50 $^\circ$) for UHPC.

ϵ: Plastic potential eccentricity, it is a small positive value which expresses the rate of approach of the plastic potential hyperbola to its asymptote. It is recommended to assume ϵ = 0.1 in the CDP model (Kmiecik and Kamiński, 2011).

F_{b0}/f_{c0}: is the proportion of initial uniaxial compressive yield stress and initial uniaxial compressive yield stress (Kmiecik and Kamiński, 2011). The default value in ABAQUS is (1.16) for NSC and UHPC.

K: is the ratio of the second stress invariant in the tensile meridian to compressive meridian for any defined value of the pressure invariant at initial yield. It is used to define the multi-axial behavior of concrete and is ($0.5<K_c\leq1$).The default value in ABAQUS is (0.667) for NSC and UHPC.

μ: is the viscosity parameter. It does not affect the ABAQUS/Explicit analysis but contribute to converge in an ABAQUS/Standard analysis. According to (Malm) (Malm, 2006) μ=10-5 for NSC and UHPC is recommended because in comparison with characteristic time increment it should be small.

A.3 Uniaxial Behavior of UHPC

A.3.1 Uniaxial Compression Behavior for UHPC

Behavior of normal concrete and high compressive strength concrete under loads is different from behavior of UHPC because of its ductility and its high strength against compressive load as well as tensile load for UHPC. Many studies about mechanical properties of UHPC, were conducted but there are very few studies

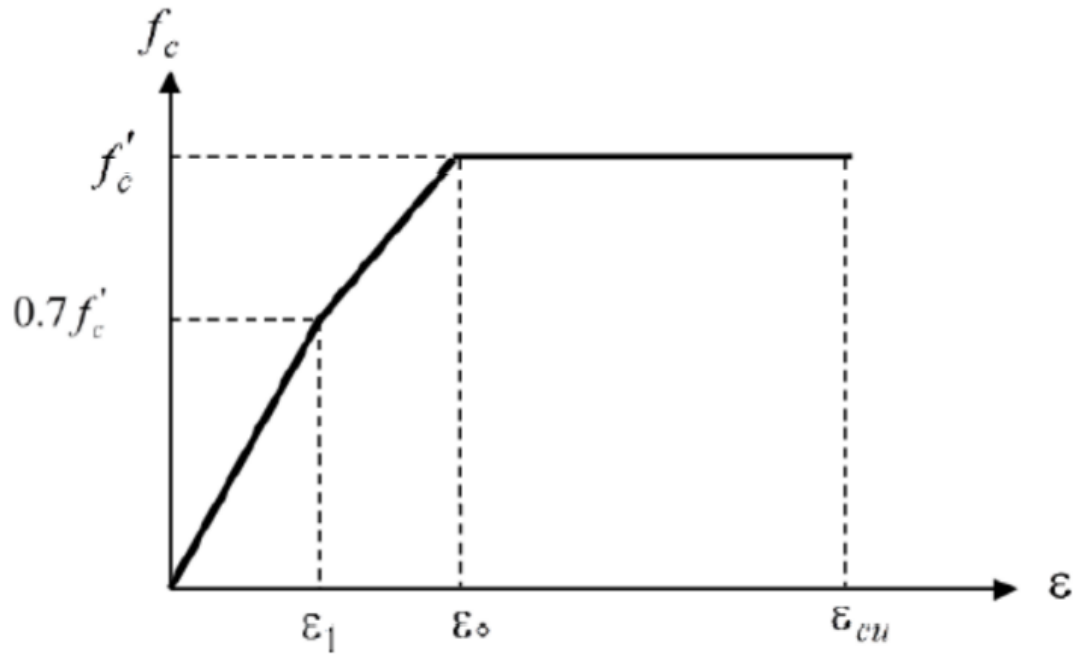described the behavior of UHPC table A-1 show the used values of stress-strain.

Figure A- 1 Typical Stress-Strain Diagram for UHPC under Uniaxial Compression.

Table A-1 values of stress–strain curves of concrete under uniaxial Compression.

fc,r (N/mm2)	118.6	119.6	119.4	110	95	76	56	39	26	16.8	10.7	6.7
$\varepsilon c,r$ (10^{-6})	246	320	426	740	1183	1721	2277	2777	3184	3498	3740	3931

Zheng et al. (Zheng et al., 2012)found that for UHPC, the strain at peak stress (ϵ_o) ranges from 0.004 to 0.005, while ultimate strain) ranges from 0.006 to 0.0075.

In the present study, the compression stress-strain relationship for UHPC can be idealized by a multilinear isotropic stress-strain curve Figure (A-1). Values that found by (Hannawayya) (Al-Hassani et al.) for UHPC are adopted in the present finite element analysis, (ϵ_o =0.0044, ϵ_o =0.0063).

A.3.2 Uniaxial Tensile Behavior for UHPC

Stress-strain relationship of UHPC with strain rate effects in tension as shown in Figure (A-2), calculated using the tensile stress-crack opening relationship of UHPC, which proposed by Fujikake et al. (Fujikake et al., 2006) as presented in
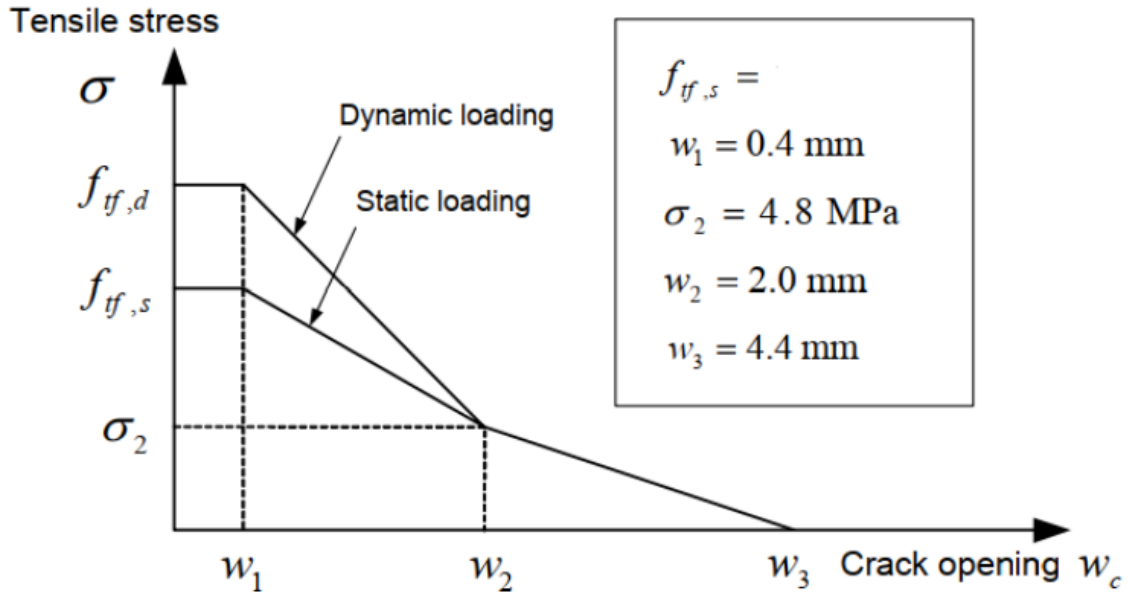
table A-2:

Table A-2 values of stress–strain curves of concrete under uniaxial tension.

ft,r (N/mm2)	12.45	11.24	10.65	9.81	8.95	7.58
εt,r (10^-6)	0	126	240	560	1480	3390

A.4 Material Properties for FEM

A.4.1 Concrete Model Properties

Figure A- 2 Typical Stress-Strain Diagram for UHPC under Uniaxial tensile.　el that should be used are: the modulus of elasticity E_o, the Poisson's ratio v and the compressive and tensile strengths of concrete In order to simulate concrete with

normal compressive strength, the unconfined stress–strain relationship model for concrete as proposed by (Popovics) (Popovics, 1973) was used. This relationship based on the concrete cylinder strength, as described in equations (A-1) and (A-2).

$$\frac{fc}{fc\prime} = \frac{n * \left[\frac{\varepsilon_c}{\varepsilon_{co}}\right]}{(n-1) + \left[\frac{\varepsilon_c}{\varepsilon_{co}}\right]^n} \qquad \text{A- 1}$$

$$n = (0.4 * 10^{-3} * fc\prime(Psi)) + 1.0 \qquad \text{A- 2}$$

Where:

$fc\prime$ = the compressive strength of cylinder at maximum stress.

ε_o = strain of concrete at maximum stress,

n = a curve − fitting factor.

On the other hand, tensile stress-strain (σ-ε) relationship was assumed linear up to the uniaxial tensile strength and then determined using the exponential function in the equation (A-3).

$$\sigma = f_t * \left[\frac{\varepsilon_t}{\varepsilon}\right]^{0.7 + 1000\varepsilon} \quad \varepsilon_t = \frac{f_t}{E_o} \qquad \text{A- 3}$$

A.4.2 Steel Reinforcement Model Properties

The required input parameters for material definition of steel bars, includes density, elastic and plastic behavior. Elastic behavior of steel material is defined by specifying Young's modulus (E_s) and Poisson's ratio (v) of which typical values are 200000 MPa and 0.3, respectively. Plastic behavior is defined in a tabular form, included yield stress and corresponding plastic strain. According to (Hibbit et al.).true stress and logarithmic strain should be defined. Input values of stress in each point for an isotropic material are calculated according to Eqs. (A-4) and (A-5). A higher number of input points lead to results that are more accurate.

$$\sigma_{true} = \sigma_{nominal}(1 + \varepsilon_{nominal}) \qquad \text{A- 4}$$

$$\sigma_{in}^{pl} = \ln(1 - \varepsilon_{nominal}) - \left(\frac{\sigma_{true}}{E_s}\right) \qquad \text{A- 5}$$

A.4.3 Steel Plate Model Properties

The steel plates were modelled using an isotropic linear elastic material model by Eq. (A-5) with solid elements for all models. The assumption for the material of loading and supporting plates is to avoid problems in solution due to the large deformations that will be developed or stress singularity in the plates.

$$f_s = E_s \varepsilon_s (MPa), \varepsilon_s \leq \varepsilon_y \qquad\qquad \text{A- 6}$$

الخلاصة

في هذه الدراسة ، تم فحص سلوك احتكاك القص للخرسانة فائقة الأداء نظرياً وعمليًا عن طريق إجراء اختبارات على 9 عينات. الخرسانة فائقة الأداء هي فئة جديدة من الخرسانة تمتاز بعدم وجود الركام الخشن، إضافة إلى وجود الالياف الفولاذية، وتكون نسبة الماء إلى الأسمنت قليلة، وذات نفاذية منخفضة. مقاومة الانضغاط لهذا النوع من الخرسانة تتجاوز ال 120 نيوتن/ ملم^2، وقوة الشد تتراوح بين 8الى 17 نيوتن / ملم^2. من أجل استخدام الخرسانة فائقة الأداء بكفائة في المفاصل الانشائية من الضروري إنشاء توصيات جديدة لأستخدامها. إن التداخل بين الخرسانة فائقة الأداء يجب ان يحدد بمحددات من اجل الاستخدام الامن لهذه الخرسانة. في هذه الدراسة تم فحص سلوك احتكاك القص من الناحية العملية و النظرية عن طريق فحص 9 نماذج. من أهم الأمور التي تم اخذها بنظر الاعتبار هو نوع التداخل وكذلك استخدام قضبان التسليح. من العوامل التي تم دراستها والتي تؤثر على احتكاك القص في المفاصل الانشائية هي قوى القص، شكل الفشل، والاستجابة لفحص القوة-الهطول. اظهرت الدراسة أن الزيادة في قضبان التسليح الخاص بالقص تعمل على تحسين مقاومة القص، كما ان وجود الاخاديد التي تربط أجزاء النموذج يحسن من قدرة الخرسانة على مقاومة القص. بينما اظهرت النماذج التي تعرضت للمعالجة بواسطة المياه النفاثة ليست فعالة في تحسين مقاومة القص. تم استخدام نظرية العناصر المحددة بأستخدام برنامج الاباكوس لإنشاء النماذج الخاصة بمقاومة احتكاك القص. اظهرت النتائج أن هناك توافق جيد بين النتائج العملية و النظرية من حيث قدرة التحميل القصوى, اضافة إلى الهطول الأقصى حيث بلغ متوسط الفرق في سعة التحميل القصوى (7.56)%. تم اقتراح عوامل جديدة ليتم فحصها نظريا مثل عدد قضبان التسليح و زيادة مقاومة الانضغاط للخرسانة. اوضحت النتائج أن زيادة قضبان التسليح من واحد إلى اثنين ومن ثلاثة إلى أربعة أدى إلى زيادة سعة التحميل القصوى بنسبة (23 و14)% تواليا مقارنة من النماذج ذات قضبان التسليح الواحدة و الثلاثية. اضافة إلى ذلك أدت زيادة مقاومة الانضغاط من (120 إلى 200) نيوتن/ملم إلى الحصول على سعة تحميل قصوى أعلى بنسبة (59و60)% للنماذج ذات الاخاديد المستطيلة والدائرية. أخيرا ثم اقتراح معادلة لحساب قوى احتكاك القص والخاصة بالخرسانة فائقة الأداء اعتمادا على النتائج العملية.

جمهورية العراق

وزارة التعليم العالي و البحث العلمي

جامعة كربلاء

كلية الهندسة

قسم الهندسة المدنية

قوة احتكاك القص لمفاصل البناء الخرسانية عالية الأداء

رسالة مقدمة الى مجلس كلية الهندسة / جامعة كربلاء وهي جزء من متطلبات نيل درجة الماجستير في علوم الهندسة المدنية

كتبت بواسطة:

علي احمد عبد الرضا

باشراف :

أ.م.د. بهاء حسين محمد

أ.د. سجاد عامر حمزة

رمضان 2023   **نيسان 2023**